ABSTRACT

DACUS, ROBERT WARREN. Development of an Adaptive Thermal Conductivity Modeling Capability. (Under the direction of Paul Turinsky.)

This thesis presents a study of a generalized perturbation theory approach to determining the difference in the values of a Quantity of Interest (QoI) as predicted by two physics models. This is accomplished by forming an inner product of a generalized adjoint solution for one model with its respective residual formed from that model's operators acting upon the other model's determined solution. This study supports the development of an adaptive model refinement capability where the value of the QoI is used to decide among models of various fidelity levels satisfying accuracy requirements.

The specific application for this thesis is the modeling of the temperature profile of a single nuclear reactor core fuel pin of ceramic uranium oxide. The fuel pin has a radius of 0.3325 inches and height of 150 inches. It is assumed to deposit heat by conduction into a closed flow channel of water surrounding the fuel. The low fidelity model chosen utilizes a finite difference model with coarse spatial meshing whereas the high fidelity model employs finer spatial meshing. Lumped parameters are used for the low fidelity model's heat transfer coefficients. Several alternative adjoint methods were developed to estimate the difference in high and low fidelity fuel temperatures. These adjoint methods include mathematical, physical, and analytical types as derived from their respective equations. The associated high fidelity adjoint solutions were found to accurately predict fuel pin temperature differences for cases where the low fidelity solution was assumed constant due to equivalent forward problem high fidelity residual values. The physical and analytical adjoint solutions were unable to predict temperature differences for cases where spatial derivatives of the low fidelity temperatures were not equal to zero. In all cases, usage of the low fidelity adjoint solution in place of the high fidelity adjoint solution resulted in inaccurate predictions of temperature differences, while the high fidelity mathematical adjoint was able to predict differences exactly at every axial and radial location.

Development of an Adaptive Thermal Conductivity Modeling Capability

by
Robert Warren Dacus

A thesis submitted to the Graduate Faculty of
North Carolina State University
in partial fulfillment of the
requirements for the Degree of
Master of Science

Nuclear Engineering

Raleigh, North Carolina

2014

APPROVED BY:

Michael Doster	Sharon Lubkin
Troy Becker	Paul Turinsky Chair of Advisory Committee

DEDICATION

To my family and dear friends.

BIOGRAPHY

The author was born in Nashville, TN to Linda and Tad Dacus, later moving to Chattanooga, TN. He completed his undergraduate degree at the University of Tennessee at Chattanooga in chemical engineering. He moved to Raleigh, NC in order to pursue his Ph.D. in nuclear engineering from North Carolina State University under the direction of Paul Turinsky.

ACKNOWLEDGEMENTS

I would like to thank my advisor, Paul Turinsky, for his patience and help with this difficult and elusary project. I would also like to thank the Rickover Fellowship staff and coworkers at both Knolls Atmoic Power Lab (KAPL) and the nuclear engineering department at NC State for their willingness to listen and offer advice in technical and non-technical areas alike. Finally, my family and friends were instrumental in supplying the much needed moral support necessary to complete this degree.

TABLE OF CONTENTS

LIST OF TABLES

LIST OF FIGURES

Chapter 1

Introduction

In computational engineering, there is always a tension between being able to predict a physical phenomenon with the highest accuracy while maintaining a reasonable computational resource requirement. Oftentimes, the interests of accuracy and CPU resource demand are directly opposed, and designers find themselves sacrificing one advantage for another. In some cases, higher fidelity models are only necessary for problems with complex geometry or rapid transients, while at other times low fidelity models offer acceptable resolution for predicting spatial or temporal behavior.

Thermal hydraulic predictions of flow regimes within nuclear reactor cores require significant computational resources and accuracy to ensure that the core design does not violate the thermal limits of involved materials. These predictions often sacrifice accuracy for efficiency or vice versa. Fluid models like direct numerical simulation (DNS) resolve flow field phenomena at the smallest physical and temporal length scales. These simulations are able to deterministically calculate velocity and pressure fields of turbulent flow but at an extreme computational cost. Other models such as Reynolds Average Navier Stokes (RANS), using turbulence models, are able to approximate system wide pressures and velocities but are unable to determine local eddy configurations on the scale of DNS. In many cases, these turbulence approximations and averaging techniques are all that is needed for simple problems such as channel flow. However, for complex geometry, it is oftentimes desired to resolve smaller length scales in order to understand and simulate appropriate thermal hydraulic behavior at, for example, downstream locations from assembly grid spacers with mixing vanes.

Even for less sophisticated methods like drift-flux or homogeneous equilibrium mixture modeling, there can still be a significant trade off between computational demand and accuracy. Ideally, a model would exist that could actively switch between higher and lower fidelity

problems such that it would employ levels of fidelity where appropriate in order to save computational resources and improve accuracy at respective locations of interest. This approach is referred to as Adaptive Model Refinement (AMoR) and has the potential of capitalizing on the accuracy and CPU resource advantages of high and low fidelity models during a single simulation. In order to employ AMoR techniques, there must be a way to estimate the differences between predicted values for the high and low fidelity models such that the computational resource requirement for the prediction still remains less than the requirement for the high fidelity model. If the adaptation algorithm exceeds the high fidelity model CPU requirement, then the advantage of using the CPU efficient low fidelity model is lost. In a related field, AMoR techniques have been shown by Jackson, Cacuci, and Finnemann to produce accurate results using three fidelity levels for nuclear reactor safety transients that require only 30% to 70% of the CPU time needed using the highest fidelity level. [1], [2].

This masters thesis project examines an adaptive model refinement approach using adjoint methods for predicting differences between high and low fidelity models and its potential application to thermal hydraulic simulations. The focus of the work is on the generalized adjoint equations formulation. What follows is a rigorous derivation of all mathematics pertaining to the investigated adaptive model refinement method as well as an investigation of the numerical results from using this method with application to a heat conduction and convection model for a single fuel pin within a fuel assembly.

1.1 Thermal Hydraulic Design and Simulation

For safe and efficient operation of a thermal nuclear power core, a fluid must effectively cool the reactor core to appropriate temperatures in order to maintain the functional integrity of materials without compromising the configuration necessary to sustain a self-propagating chain reaction of the nuclear fuel. It is necessary for designers to understand the behavior of system wide pressures and velocities and how they affect overall plant performance as well as local fluid behavior that can influence things like corrosion and neutron flux. A wide variety of numerical tools is necessary in order to properly design and simulate a nuclear reactor and its plant and safety components. Each tool essentially presents a solution or approximation of the three dimensional mass, momentum, and energy balance equations for single or multiphase fluid flow. The level of simplification and estimation of these equations coincides with the demand for accuracy that a designer requires to predict a specific quantity of interest.

One dimensional or three dimensional techniques for solving the two phase mixture equa-

tions are typical for basic system wide simulation. Design codes such as RELAP and TRAC implement these methods for best-estimate thermal hydraulic design [19], [20]. Correlations are chosen in order to close the six-equation two phase system describing the mass, momentum, and internal energy of a flow field. For simulation and analysis focused on core internal thermal hydraulic behavior, either closed-channel methods or sub-channel methods as incorporated by COBRA and VIPRE codes are employed [21], [22]. The two-phase drift flux model, which considers only mixture momentum instead of separate phasic momentum equations and uses a correlation for determining the relative velocity of phases, may be employed for similar simulation conditions. Alternatively, the homogeneous equilibrium mixture (HEM) model assumes that both phases are at saturation and moving at the same velocity; therefore one only needs to solve for mixture momentum, mass, and energy. Although these methods are fast, they typically are unable to resolve flow mechanics close to the wall of the system, where oftentimes safety criteria such as critical heat flux (CHF) are a concern.

For simulating the wall resolved effects of turbulent flow, various computational multiphase fluid dynamics (CMFD) methods can be used to investigate flow phenomena that cannot be resolved by using simplified equations. In most cases momentum, mass, and energy are solved explicitly for each phase. Equations for turbulent kinetic energy and turbulent dispersion are also necessary in order to describe the effect of turbulence on the flow regime. Models such as k-ϵ or k-ω are typical for RANS equations and use correlations to describe the velocity distribution near the wall. As a consequence, the averaging technique used by RANS loses information regarding small eddy formation and dissipation within the flow field. Large eddy simulation (LES) can be used in its stead in order to retain the turbulence induced time dependent perturbation in the flow field. However, this is often computationally limiting due to the need for finer spatial meshing and time dependent ensemble average solutions. Codes such as STAR-CCM+ and HYDRA-TH enable RANS and LES methods to be used, employing a multiphase, N-field model [23], [24].

DNS methods mentioned previously have the capability of resolving all micro scales of fluid flow. These methods employ a variety of techniques for tracking the interface between liquid and vapor. Examples are front tracking and level set methods which both have the capability of simulating individual bubble or droplet interaction within a fluid. In this case, no wall models or correlations are necessary due to the fact that the length scale of individual bubbles has been resolved. The computational resources needed to implement these methods for a single reactor core channel containing thousands of bubbles are vast and DNS techniques are not typically used for large scale design. The computational codes PHASTA and FTC3D employ these DNS methods [25], [26]. They have proven useful for gaining insights and developing closure rela-

tionships for LES and RANS models, e.g. bubble lift and drag forces.

Each of the aforementioned fluid simulation techniques have advantages and disadvantages in terms of accuracy and computational resource requirement. Depending on the level of resolution required at the wall of a channel or whether full system response phenomena is of interest, designers will choose a model which exhibits a level of accuracy analogous with their design requirements.

All of these fidelity levels are used in concert with one other to ensure proper design of a nuclear reactor core and its supporting thermal hydraulic systems. Within each method, various closure models or equation parameters can help improve the physical accuracy of the problem at the cost of additional computational resources. In some cases though, the fidelity required at one point in the problem's geometry may not be necessary at other parts of the problem and the resulting computational requirement of using the higher fidelity model for the entire geometry may prove burdensome.

1.2 Adjoint Methods

Adjoint problems are mathematical constructs that mirror behavior found in physical or forward problems and help describe the importance of functionals with respect to a specific quantity of interest. Adjoint methods have found widespread use in the field of radiation transport due to its usefulness in perturbation analysis [1] - [3]. For small changes in specific parameters, adjoint solutions can describe the influence that these changes have within the detection region of interest. In neutronics, these changes can include material properties, source distributions, and cross sections. In thermal hydraulics, these changes include material properties as well as heat conduction estimations for inverse problems [4] - [8].

In computational fluid dynamics (CFD - single phase fluids as opposed to CMFD), adjoint methods are often used for adaptive grid refinement. These methods provide error controlled localized grid refinement as an attempt to reduce the numerical error present in CFD methods. Refining the grid needlessly does not explicitly reduce the numerical error, and there is a need to understand where and when grid refinement improves accuracy in order to maximize the efficiency of the refinement. Adjoint solution shapes can be thought of as importance weighting functions, and they can be used to quantify the importance of functionals like lift or drag within specific geometric locations of the spatial grid. Analysts can then use this information to determine where and to what degree a grid can be improved in order to reduce the numerical

error of the functional [9].

1.2.1 Detector Example

In adjoint problems, one has the freedom to describe boundary conditions and source terms such that the evaluation of a function yields the desired quantity of interest. A simple example is the detector response problem which is applicable to both thermal hydraulics and neutronics problems. In this problem, the response of a detector is desired as a function of source location. Typically, moving the source anywhere within the geometry of the problem necessitates a new temperature or flux field solution in order to evaluate detector response. Adjoint methods present an alternative approach.

Starting with the following forward and adjoint linear equations

$$A\left[\phi\right] = Q, \qquad A^*\left[\phi^*\right] = Q^* \tag{1.1}$$

the adjoint operator A^* is defined such that the following inner product equality holds for all ϕ and $\phi*$ within the solution space

$$\left\langle A\left[\phi\right], \phi^*\right\rangle = \left\langle A^*\left[\,\phi^*\,\right], \phi\right\rangle \tag{1.2}$$

Ensuring equality of (1.2) imposes restrictions on the boundary conditions of the adjoint problem. If the response function desired is defined as $R = \langle \Sigma, \phi \rangle$ then one can provide an exact evaluation of the response when the adjoint source term is given by $Q^* = \Sigma$

$$\langle \Sigma, \phi \rangle = \langle Q^*, \phi \rangle = \langle A^*[\phi^*], \phi \rangle = \left\langle A\left[\phi\right], \phi^*\right\rangle = \langle Q, \phi^* \rangle \tag{1.3}$$

Using (1.3), one is able to determine the response of a detector for various Q locations without having to solve for ϕ each time Q is moved. Instead, ϕ^* is determined once and then can provide the response for any value of Q in the solution space. This method of functional response prediction with respect to adjoint solutions can provide a means for performing adaptive model refinement with application to simple fuel conduction and convection problems investigated by this thesis.

1.2.2 Physical and Mathematical Adjoint Operators

There are two distinct methods for deriving the adjoint A^* operator. A physical adjoint is defined as an adjoint operator that is derived from the continuous set of forward equations. One constrains the adjoint operator in order to satisfy equation (1.2) and, using integration by parts,

comes to an appropriate adjoint operator. The application of appropriate boundary conditions (generally homogeneous) ensures that the equality in (1.2) holds.

Each forward operator present in a set of equations will have a corresponding adjoint operator. These operators are said to be self adjoint if $A^* = A$. Second derivatives and constant multipliers are examples of self adjoint operators while first order derivatives are not self adjoint [1]. Adjoints of matrix operators can be derived as well by taking the conjugate transpose of the original matrix.

Discrete adjoint solutions can be found by solving for the discretized set of adjoint equations as derived from the forward equations. This adjoint problem is referred to in this work as a physical adjoint.

Another method of arriving at a set of discretized adjoint equations is to derive them from the discretized forward equations. Since the adjoint of a matrix operator is the conjugate transpose of the matrix, then for a discretized forward matrix $\bar{\bar{\mathbf{A}}}$ operating on the forward solution vector $\bar{\phi}$, we have the following forward and adjoint problem

$$\bar{\bar{\mathbf{A}}}\left[\bar{\phi}\right] = \bar{\mathbf{Q}}, \qquad \bar{\bar{\mathbf{A}}}^{\mathbf{T}}\left[\bar{\phi}^*\right] = \bar{\mathbf{Q}}^* \tag{1.4}$$

This method requires no integration by parts, and the appropriate boundary and initial conditions for the adjoint problem are embedded in the transposed matrix $\bar{\bar{\mathbf{A}}}^T$. In this work, the previously defined adjoint problem is referred to as the mathematical adjoint. As the time and spatial discretization steps approach zero, the discrete mathematical adjoint equations are expected to approach the physical adjoint equations. For discrete problems, there is no guarantee that the discretized physical adjoint solution will be the same as the mathematical adjoint solution. However, if the problems are defined correctly, the functional as predicted by the adjoint solutions should be the same for both the physical and mathematical problems.

1.3 Problem Definition

1.3.1 Forward Problem

This forward problem models one dimensional heat conduction through a cylindrical fuel pin of uranium oxide. This fuel pin has a radius of 0.3325 inches and a height of 150 inches. It is assumed to deposit heat directly into a channel of water surrounding the fuel. The heat generation can either vary sinusoidally in the axial direction and is constant in the radial direction or is constant in all directions. The coolant model assumes that the steam and liquid are both

have the same pressure and velocity, and have temperatures that vary in the axial direction. The equation set, initial conditions, and boundary conditions below model the fuel conduction and convection of a cylindrical fuel pin.

$$c_p^f \rho_f \frac{\partial}{\partial t} T_f - k_f \nabla_r^2 \, T_f = q''' \tag{1.5}$$

$$c_p^c \rho_c A_x \frac{\partial}{\partial t} T_c + c_p^c \dot{m}_c \frac{\partial}{\partial z} T_c + S_f k_f \nabla_r \, T_f|_{r=R} = 0 \tag{1.6}$$

$$h_c \left(T_f|_{r=R} - T_c \right) = -k_f \nabla_r \, T_f|_{r=R} \tag{1.7}$$

$$T_c|_{t=0} = T_c^{(o)} \qquad T_f|_{t=0} = T_f^{(o)} \tag{1.8}$$

$$T_c|_{z=0} = T_c^{In} \qquad \nabla_r \, T_f|_{r=o} = 0 \tag{1.9}$$

where T_f is the fuel temperature as a function of time t, axial location z, and radial location r; T_c is the coolant temperature as a function of time t and axial location z. Heat energy generated, denoted by the z dependent variable q''', conducts radially through the pin. Axial heat conduction is ignored, however T_f is still z dependent. This dependency arises from the axial coupling present in equation (1.7) which describes heat convection along the outside surface of the pin. All heat generated in the pin by the q''' term is conducted to the outside surface and passes into the coolant and out the exit boundary condition at the top of the channel. Fluid flow properties are represented by a single mass flow rate term $\dot{m}_c$ where closed flow channel, single phase, and constant density are assumed to make the flow rate constant with z.

Figure 1.1 contains a visual representation of the cylindrical UO_2 fuel pin and its respective radial and axial discretization. There are 4 radial cells or rings and 4 axial meshes shown in the figure. Each fuel and coolant temperature location, denoted by $T_{f-i,j}$ and T_{c-j} respectively with $i \in [1, 2, ..., N_r]$ and $j \in [1, 2, ..., N_z]$, is shown along with its node number, denoted by ϕ_l with $l \in [1, 2, ..., N_l]$ where N_l represents the total number of discretized cells. Again, $\bar{\boldsymbol{\phi}}$ is the solution vector containing all fuel and coolant temperatures. The cell numbering starts at the center radial cell of the first axial mesh and then increases as it moves in the positive r direction. Upon reaching the outer most radial cell, the numbering drops below to the next axial mesh, center radial ring and increases in node number as r increases. The coolant temperature nodes are at the end of the $\bar{\phi}$ vector, starting at the top axial mesh and moving downward.

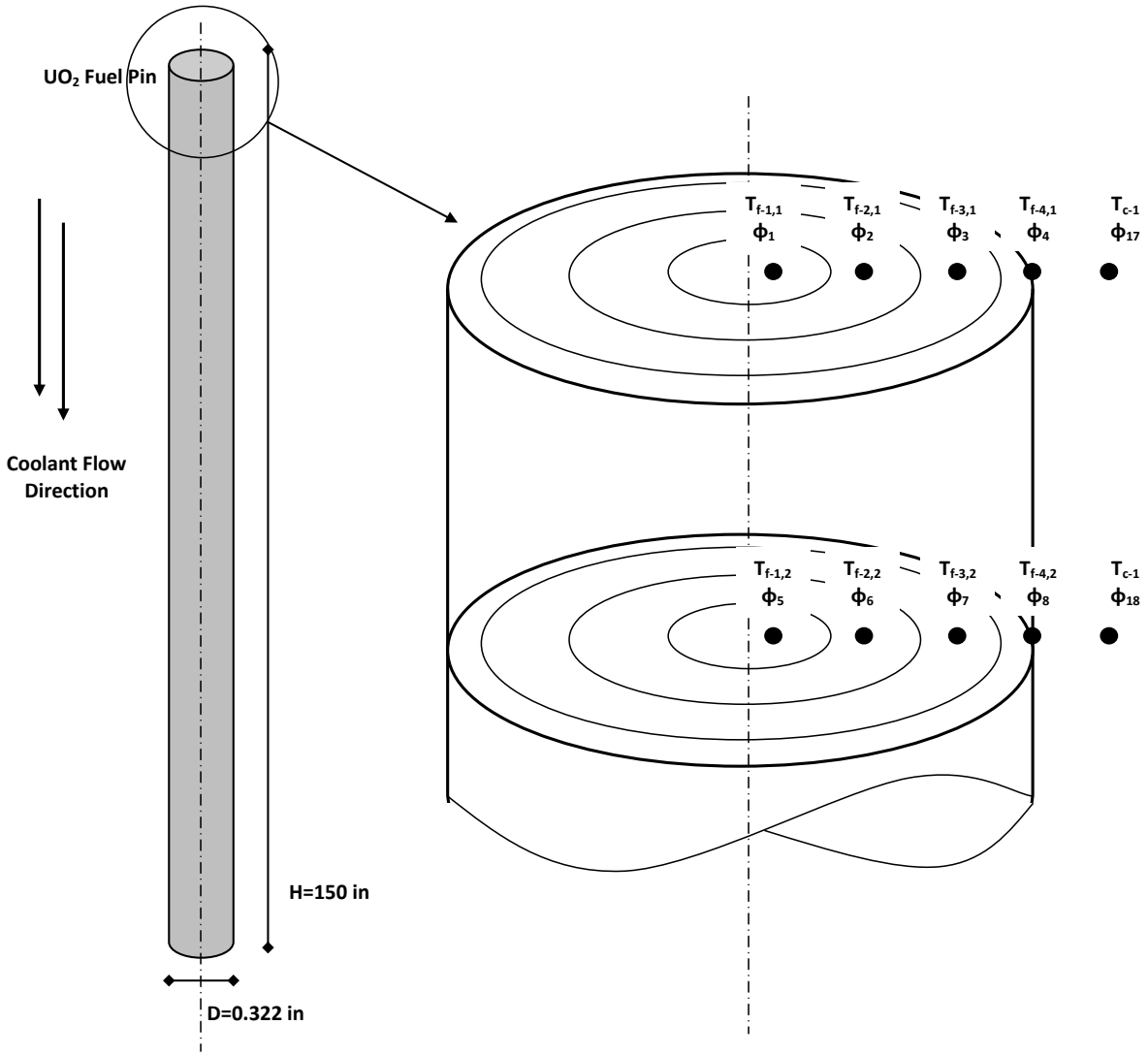

$$\overline{\phi} = \left[\phi_1 \;\; \phi_2 \;\; \phi_3 \;\; \phi_4 \cdots \phi_{17} \;\; \phi_{18} \;\; \phi_{19} \;\; \phi_{20}\right]^{\mathrm{T}}$$

Figure 1.1: **Physical geometry of simplified forward problem and example discretization and node numbering**

The gradient and Laplacian operators, ∇_r and ∇_r^2 respectively, denote the use of cylindrical coordinates. Table 1.1 contains a list of constants and their values used for the high fidelity forward problem. These values are assumed to remain constant regardless of material temperature for the high fidelity case. In the low fidelity case, k_f and h_c are adjusted in order to conserve the heat flux between collapsed discretized radial mesh cells, simply refered to as rings throughout this thesis.

Table 1.1: **Physical properties for fuel pin equations**

Property	**Symbol**	**Value**
Fuel Specific Heat	c_p^f	0.0762 BTU/lbm-F
Coolant Specific Heat	c_p^c	1.394 BTU/lbm-F
Fuel Thermal Conductivity	k_f	2.00 BTU/hr-ft-F
Fuel Density	ρ_f	685 lbm/ft^3
Coolant Mass Flow Rate	$\dot{m}_c$	3124 lbm/hr
Coolant Convection Coefficient	h_c	8,500 BTU/hr-ft$^2 - F$
Coolant Flow Area	A_x	0.174 in^2
Fuel Pin Radius	R	0.161 in
Fuel Pin Circumference	S_f	1.013 in

Equations (1.5) and (1.6) are solved using two separate levels of discretization. The high fidelity model employs a finite difference model for approximating both radial and axial derivatives. The low fidelity problem uses lumped parameters in order to determine material conductivities of the fuel and coolant. It also uses finite difference to approximate derivatives with fewer radial rings as compared to the high fidelity model. The number of axial nodes remains constant and equal for both the high fidelity and low fidelity simulations.

Additionally, for q'''constant, there is a simple analytical solution to the forward continuous equation set. This can be used to verify the discrete numerical solution for the high fidelity forward problem. Additionally, this analytic solution can be used in conjunction with the adjoint analytical solution to verify the continuous adjoint's evaluation of a functional. The analytic solution provides insight into the ability of low fidelity adjoints for use in the approximation of functional values. The discrete high and low fidelity models and continuous forward model are investigated rigorously in the derivation section of this thesis.

1.3.2 Adjoint Problem

Three adjoint problems are considered with application for adaptive model refinement. These are referred to as the mathematical, physical, and analytic adjoint models respectively. The adjoint equation set, final conditions, and boundary conditions presented below are derived from the forward continuous equations (1.5) - (1.9)

$$-\rho_f \frac{\partial}{\partial t} T_f^* - k_f \nabla_r^2 T_f^* = Q^* \tag{1.10}$$

$$c_p^c \rho_c A_c \frac{\partial}{\partial t} T_c^* + c_p^c \dot{m}_c \frac{\partial}{\partial z} T_c^* = S_f k_f \nabla_r \, T_f^* \big|_{r=R} \tag{1.11}$$

$$-k_f \nabla_r T_f^* \big|_{r=R} = h_c \left(T_f^* \big|_{r=R} - T_c^* \right) = q''^* \big|_{r=R} \tag{1.12}$$

$$T_c^* \big|_{t=t_F} = \quad T_f^* \big|_{t=t_F} = 0 \tag{1.13}$$

$$T_c^\dagger \Big|_{z=H} = 0, \quad \nabla_r \, T_f^\dagger \Big|_{r=0} = 0 \tag{1.14}$$

with t_f denoting the final time. This equation set is referred to as the analytic adjoint and is derived rigorously in the following section. Q^* varies according to the problem definition and the quantity of interest to be evaluated by the response. For certain Q^*, this equation set admits an analytic solution.

Similar to the analytic forward solution, the analytic adjoint solution presents a continuous solution to the simplified adjoint problem for use in verifying the physical and mathematical adjoint results. The physical adjoint refers to the discretized version the above equation set using finite difference in the same manner as the high fidelity forward problem.

Another method for arriving at a discretized adjoint is to take the conjugate transpose of the forward matrix operator. The time dependent forward problem can be described by the following matrix equation

$$\bar{\bar{\mathbf{C}}}_{\mathbf{n+1}} \bar{\boldsymbol{\phi}}_{\mathbf{n+1}} = \bar{\bar{\mathbf{B}}}_{\mathbf{n+1}} \bar{\boldsymbol{\phi}}_{\mathbf{n}} + \bar{\mathbf{Q}}_{\mathbf{n+1}} \tag{1.15}$$

where $n+1$ is the current timestep, n is the previous timestep, and the $\bar{\bar{\mathbf{C}}}$ and $\bar{\bar{\mathbf{B}}}$ are matrix operators acting on the appropriate time dependent solution vector $\bar{\boldsymbol{\phi}}$. Equation (1.15) can be written in block matrix form as

$$\begin{bmatrix} \bar{\bar{\mathbf{C}}}_{\mathbf{1}} & & & \\ \bar{\bar{\mathbf{B}}}_{\mathbf{2}} & \bar{\bar{\mathbf{C}}}_{\mathbf{2}} & & \\ & \bar{\bar{\mathbf{B}}}_{\mathbf{3}} & \bar{\bar{\mathbf{C}}}_{\mathbf{3}} & \\ & & \ddots & \ddots \end{bmatrix} \begin{bmatrix} \bar{\phi}_1 \\ \bar{\phi}_2 \\ \bar{\phi}_3 \\ \vdots \end{bmatrix} = \begin{bmatrix} \bar{\mathbf{Q}}_1 \\ \bar{\mathbf{Q}}_2 \\ \bar{\mathbf{Q}}_3 \\ \vdots \end{bmatrix}$$

which can be explicitly solved for a given set of initial conditions. The time dependent mathematical adjoint is then simply the conjugate transpose of this block matrix structure and each individual matrix operator. Similar to the analytic forward solution, the analytic adjoint solution admits a continuous solution to the simplified adjoint problem for use in verifying the physical and mathematical adjoint results. Therefore, one has for the mathematical adjoint problem

$$\begin{bmatrix} \bar{\bar{\mathbf{C}}}^*_{\mathbf{1}} & \bar{\bar{\mathbf{B}}}^*_{\mathbf{2}} & & \\ & \bar{\bar{\mathbf{C}}}^*_{\mathbf{2}} & \bar{\bar{\mathbf{B}}}^*_{\mathbf{3}} & \\ & & \bar{\bar{\mathbf{C}}}^*_{\mathbf{3}} & \ddots \\ & & & \ddots \end{bmatrix} \begin{bmatrix} \bar{\phi}^*_1 \\ \bar{\phi}^*_2 \\ \bar{\phi}^*_3 \\ \vdots \end{bmatrix} = \begin{bmatrix} \bar{\mathbf{Q}}^*_1 \\ \bar{\mathbf{Q}}^*_2 \\ \bar{\mathbf{Q}}^*_3 \\ \vdots \end{bmatrix}$$

which can also be explicitly solved for a given a set of final conditions. The definition of adjoint matrix operators results in

$$\bar{\bar{\mathbf{C}}}^* = \bar{\bar{\mathbf{C}}}^{\mathbf{T}}, \qquad \bar{\bar{\mathbf{B}}}^* = \bar{\bar{\mathbf{B}}}^{\mathbf{T}}$$

Chapter 2

Derivation of Forward and Adjoint Problems

The following section describes the derivation of the forward and adjoint methods used by the adaptive model refinement method for heat conduction and convection. The first section outlines the continuous and discrete high fidelity forward problem. The next section shows the derivation of adjoint equations by two separate means - formulating both the physical adjoint and a mathematical adjoint. The physical adjoint equation derives discrete adjoint equations from the continuous adjoint equations. Conversely, mathematical adjoint equations derives operators from discrete forward equations by taking the conjugate transpose of the forward linear operator. Ideally, a physical and mathematical adjoint derivation should arrive at the same set of continuous adjoint equations in the limit where time and spatial step sizes approach zero.

Due to the simplicity of the forward heat conduction and single node convection problem, it was possible under certain conditions to formulate an analytical solution for both the steady state forward and adjoint problem. One can then show explicitly that the response function of interest with regards to the adjoint solution can represent the exact quantity of interest. The final section of this chapter describes the low fidelity problem.

2.1 Forward Problem

The following section describes the forward fuel conduction and convection problem discretization for both the low and high fidelity models. Also included is a derivation of the analytic solution to the steady state problem with constant heat generation.

2.1.1 High Fidelity Discretization

In order to discretize the forward problem using finite difference methods, the steady state problem is first considered. Setting time derivatives to zero we have the following forward problem

$$k_f \nabla_r^2 T_f = q''', \qquad -c_{p_c} \dot{m}_c \frac{\partial T_c}{\partial z} + q''\big|_{r=R} = 0$$

$$-k_f \nabla_r \, T_f|_{r=R} = h_c \left(T_f|_{r=R} - T_c \right)$$

$$\nabla_r \, T_f|_{r=0} = 0, \quad T_c|_{z=0} = T_{c,in}$$

$$q''\big|_{r=R} = h_c S_f \left(T_f|_{r=R} - T_c \right)$$

Integrating the fuel equation over $\int_{r_i}^{r_{i+1}} \cdot 2\pi r \mathrm{d}r$ results in

$$k_f \int_{r_i}^{r_{i+1}} \nabla^2 T_f 2\pi r \mathrm{d}r = k_f \int_{r_i}^{r_{i+1}} 2\pi r \left(\frac{1}{r} \frac{\partial}{\partial r} \left(r \frac{\partial T_f}{\partial r} \right) \right) \mathrm{d}r$$

$$= 2\pi k_f \int_{r_i}^{r_{i+1}} \left(\frac{\partial}{\partial r} \left(r \frac{\partial T_f}{\partial r} \right) \right) \mathrm{d}r = 2\pi k_f r \left. \frac{\partial T_f}{\partial r} \right|_{r_i}^{r_{i+1}}$$

Taking the finite difference of $\dfrac{\partial T_f}{\partial r}$, assuming Δr is constant, and setting $z = z_j$ we have

$$2\pi k_f r \left. \frac{\partial T_f}{\partial r} \right|_{r_i}^{r_{i+1}} \approx 2\pi k_f \left[r_h \frac{T_{f_{h,j}} - T_{f_{h-1,j}}}{\Delta r} \right|_{h=r_i}^{h=r_i+1}$$

$$= 2\pi k_f \left[r_i \frac{T_{f_{i+1,j}} - T_{f_{i,j}}}{\Delta r} - r_{i-1} \frac{T_{f_{i,j}} - T_{f_{i-1,j}}}{\Delta r} \right]$$

$$= 2\pi k_f \left[\frac{r_i}{\Delta r} T_{f_{i+1,j}} - \left(\frac{r_i}{\Delta r} + \frac{r_{i-1}}{\Delta r} \right) T_{f_{i,j}} + \frac{r_{i-1}}{\Delta r} T_{f_{i-1,j}} \right]$$

where $r_i^+ \equiv r_i + \Delta r/2$ and $T_{f_{i,j}} \equiv T_f \left(r_i^+, z_j + \Delta z/2 \right)$.

Define the following constants for $i = (1, N_r - 1)$:

$$\mathrm{a}_i \equiv 2\pi k_f \frac{r_i}{\Delta r}$$

$$\mathrm{b}_i \equiv -\left(a_{i-1} + a_i \right)$$

Using these constants, the previous expression becomes

$$= a_i T_{f_{i+1,j}} + b_i T_{f_{i,j}} + a_{i-1} T_{f_{i-1,j}}$$

In order to evaluate the expression $2\pi k_f r \left.\dfrac{\partial T_f}{\partial r}\right|_{r_i}^{r_{i+1}}$ at the first node, the boundary condition for $\nabla_r T_f|_{r=0}$ is directly substituted resulting in:

$$2\pi k_f r \left.\frac{\partial T_f}{\partial r}\right|_{r_1}^{r_2} = 2\pi k_f r \left.\frac{\partial T_f}{\partial r}\right|_{r_2} - 2\pi k_f r \left.\frac{\partial T_f}{\partial r}\right|_{r_1}$$

$$= 2\pi k_f r_2 \left(\frac{T_{f_{2,j}} - T_{f_{1,j}}}{\Delta r}\right) = 2\pi k_f \left[\frac{r_2}{\Delta r} T_{f_{2,j}} - \frac{r_2}{\Delta r} T_{f_{1,j}}\right]$$

$$= a_2 T_{f_{2,j}} - a_2 T_{f_{1,j}}$$

At the fuel pin surface, there is a special definition for $T_{f^*_{N_r}}$ such that $T_{f^*_{N_r}} \equiv T_f\left(R, z_j + \Delta z/2\right)$. The pin edge fuel temperature, $T_f|_R$, is assumed to equal the average fuel temperature for the outermost ring. Applying this relationship to the final radial node of the fuel pin results in the following

$$2\pi k_f r \left.\frac{\partial T_f}{\partial r}\right|_{r_{N_r-1}}^{r_{N_r}} = 2\pi k_f r \left.\frac{\partial T_f}{\partial r}\right|_{r_{N_r}} - 2\pi k_f r \left.\frac{\partial T_f}{\partial r}\right|_{r_{N_r-1}}$$

$$= 2\pi R k_f \left[-\frac{h_c}{k_f}\left(T_{f^*_{N_r,j}} - T_{c_j}\right)\right] - 2\pi k_f r_{N_r-1} \left(\frac{T_{f^*_{N_r,j}} - T_{f_{N_r-1,j}}}{\Delta r}\right)$$

$$= 2\pi R h_c T_{c_j} - \left(2\pi R h_c + \frac{2\pi k_f r_{N_r-1}}{\Delta r}\right) T^*_{f_{N_r,j}} + \left(\frac{2\pi k_f r_{N_r-1}}{\Delta r}\right) T_{f_{N_r-1,j}}$$

Noting that $2\pi R = S_f$ the following constants are defined

$$f = S_f h_c$$

$$e = -\left(\mathrm{f} + \mathrm{a}_{N_r-1}\right)$$

Using these constants, the previous expression is then

$$= f T_{c_j} + e T_{f^*_{N_r,j}} + a_{N_{r-1}} T_{f_{N_r-1,j}}$$

For the coolant, we assume that Δz is uniform axially along the pin, and we define $T_{c_j} \equiv T_c\left(z_j\right)$ at the axial node position for $z_j \in [0, H]$. At $j = 0$, we have $T_{c_o} = T_c(0) = T_{c,in}$.

For the surface boundary condition of the pin we have the following expression

$$q''|_{r=R} = h_c S_f \left(T_f|_{r=R} - T_c\right) = h_c S_f \left(T_{f^*_{N_r}} - T_{c_{j+1/2}}\right) = h_c S_f \left(T_{f^*_{N_r}} - T_{c_j}\right)$$

Substituting the upwinded finite difference for $\frac{\partial T_c}{\partial z}$ at cell $j + 1/2$ results in the following

$$-c_{p_c}\dot{m}_c \frac{\partial T_c}{\partial z} + q''|_{r=R} \approx -c_{p_c}\dot{m}_c \left(\frac{T_{c_{j+1}} - T_{c_j}}{\Delta z}\right) + h_c S_f \left(T_{f^*_{N_r,j}} - T_{c_j}\right)$$

$$= \left(\frac{c_{p_c}\dot{m}_c}{\Delta z} - h_c S_f\right) T_{c_j} - \left(\frac{c_{p_c}\dot{m}_c}{\Delta z}\right) T_{c_{j+1}} + h_c S_f T_{f^*_{N_r,j}}$$

Define the following constants

$$k = -\frac{c_{p_c}\dot{m}_c}{\Delta z}$$

$$m = -\left(\mathrm{k} + \mathrm{f}\right)$$

Using these constants, the previous expression becomes

$$= mT_{c_j} + kT_{c_{j+1}} + fT_{f^*_{N_r,j}}$$

The steady state discretized problem is then

$$\bar{\bar{\mathbf{A}}}\bar{\boldsymbol{\phi}} + \bar{\mathbf{d}} = 0 \tag{2.1}$$

with $\bar{\boldsymbol{\phi}} = \left[\bar{T_f}\ \bar{T_c}\right]^T$ and, the steady state temperature operator $\bar{\bar{\mathbf{A}}}$ defined as

$$\bar{\bar{\mathbf{A}}} = \begin{bmatrix} \bar{\bar{\mathbf{D}}}_f & \bar{\bar{\mathbf{O}}}_f \\ \bar{\bar{\mathbf{O}}}_c & \bar{\bar{\mathbf{D}}}_c \end{bmatrix}$$

with

$$\bar{\bar{\mathbf{D}}}_f = \begin{bmatrix} -a_2 & a_2 & & & & & \\ a_2 & b_3 & a_3 & & & & \\ & a_3 & b_4 & a_4 & & & \\ & & & \ddots & & & \\ & & & a_{N_r-2} & b_{N_r-1} & a_{Nr-1} & \\ & & & & a_{N_r-1} & e & \\ & & & & & \ddots & \end{bmatrix}, \quad \bar{\bar{\mathbf{O}}}_f = \begin{bmatrix} \vdots & & & & \\ f & & & & \\ & \ddots & & & \\ & & f & & \\ & & & \ddots & \\ & & & & f \end{bmatrix},$$

$$\bar{\bar{\mathbf{D}}}_c = \begin{bmatrix} m & & & \\ k & m & & \\ & & \ddots & \\ & & & k \quad m \end{bmatrix}, \quad \bar{\bar{\mathbf{O}}}_c = \begin{bmatrix} \cdots & f & & \\ & & \ddots & \\ & & & f \end{bmatrix}$$

In order to solve the time dependent system, we consider the following spatially discretized system

$$\bar{\boldsymbol{\gamma}} \frac{\partial \bar{\boldsymbol{\phi}}}{\partial t} = \bar{\bar{\mathbf{A}}} \bar{\boldsymbol{\phi}} + \bar{\mathbf{d}} \tag{2.2}$$

with $\bar{\boldsymbol{\gamma}} = [c_p^f \rho_f \; c_p^f \rho_f \ldots c_p^f \rho_f]^T$. Integrate equation (2.1) over the interval $\int_{t_n}^{t_{n+1}} \cdot dt$

$$\int_{t_n}^{t_{n+1}} \left[\bar{\boldsymbol{\gamma}} \frac{\partial \bar{\boldsymbol{\phi}}}{\partial t} = \bar{\bar{\mathbf{A}}} \bar{\boldsymbol{\phi}} + \bar{\mathbf{d}} \right] dt$$

$$\bar{\boldsymbol{\gamma}} \bar{\boldsymbol{\phi}}_{n+1} - \bar{\boldsymbol{\gamma}} \bar{\boldsymbol{\phi}}_n = \int_{t_n}^{t_{n+1}} \left(\bar{\bar{\mathbf{A}}} \bar{\boldsymbol{\phi}} + \bar{\mathbf{d}} \right) dt$$

We approximate the time integration by using the following equation

$$\bar{\boldsymbol{\gamma}} \bar{\boldsymbol{\phi}}_{n+1} - \bar{\boldsymbol{\gamma}} \bar{\boldsymbol{\phi}}_n \approx \left\{ \alpha \left[\bar{\bar{\mathbf{A}}} \bar{\boldsymbol{\phi}} + \bar{\mathbf{d}} \right]_{t_{n+1}} + (1-\alpha) \left[\bar{\bar{\mathbf{A}}} \bar{\boldsymbol{\phi}} + \bar{\mathbf{d}} \right]_{t_n} \right\} \Delta t_n$$

which is an explicit or implicit time discretization with $\alpha = (0, 1)$. Reordering the previous equation results in

$$\bar{\boldsymbol{\gamma}}\bar{\boldsymbol{\phi}}_{n+1} - \alpha\Delta t_n \bar{\bar{\mathbf{A}}}_{n+1}\bar{\boldsymbol{\phi}}_{n+1} = \bar{\boldsymbol{\gamma}}\bar{\boldsymbol{\phi}}_n + (1-\alpha)\Delta t_n \bar{\bar{\mathbf{A}}}_n\bar{\boldsymbol{\phi}}_n + \alpha\Delta t_n \bar{\mathbf{d}}_{n+1}$$

This expression can be written generally as

$$\bar{\bar{\mathbf{C}}}_{n+1}\bar{\boldsymbol{\phi}}_{n+1} = -\bar{\bar{\mathbf{B}}}_{n+1}\bar{\boldsymbol{\phi}}_n + \bar{\mathbf{Q}}_{n+1} \tag{2.3}$$

with

$$\begin{aligned}
\bar{\bar{\mathbf{C}}}_{n+1} &\equiv \bar{\boldsymbol{\gamma}}\bar{\bar{\mathbf{I}}} - \Delta t_n \bar{\bar{\mathbf{A}}}_{n+1} \\
\bar{\bar{\mathbf{B}}}_{n+1} &\equiv \bar{\boldsymbol{\gamma}}\bar{\bar{\mathbf{I}}} - \Delta t_n \bar{\bar{\mathbf{A}}}_{n} \\
\bar{\mathbf{Q}}_{n+1} &\equiv \alpha\Delta t_n \bar{\mathbf{d}}_{n+1} + (1-\alpha)\Delta t_n \bar{\mathbf{d}}_n
\end{aligned}$$

This time discretization structure results in a block matrix similar to the one presented in the previous mathematical adjoint example.

$$\begin{bmatrix}
\bar{\bar{\mathbf{C}}}_{\mathbf{1}} & & & \\
\bar{\bar{\mathbf{B}}}_{\mathbf{2}} & \bar{\bar{\mathbf{C}}}_{\mathbf{2}} & & \\
 & \bar{\bar{\mathbf{B}}}_{\mathbf{3}} & \bar{\bar{\mathbf{C}}}_{\mathbf{3}} & \\
 & & \ddots & \ddots
\end{bmatrix}
\begin{bmatrix} \bar{\boldsymbol{\phi}}_1 \\ \bar{\boldsymbol{\phi}}_2 \\ \bar{\boldsymbol{\phi}}_3 \\ \vdots \end{bmatrix}
=
\begin{bmatrix} \bar{\mathbf{Q}}_1 \\ \bar{\mathbf{Q}}_2 \\ \bar{\mathbf{Q}}_3 \\ \vdots \end{bmatrix}$$

The above system of equations can be solved given an appropriate set of initial conditions.

2.1.2 Low Fidelity Problem

The low fidelity problem is roughly the same as the high fidelity problem but with fewer radial rings. Adjusted values for thermal conductivities are used in the low fidelity problem such that the volume averaged temperatures for the high fidelity solution are equivalent to the low fidelity solution. This resulting low fidelity solution must then be mapped onto the high fidelity mesh in order to evaluate the high fidelity residual used with the adjoint to evaluate the difference metric. The current mapping method is simple linear interpolation between low fidelity node solutions. Figure 2.1 below shows a representative grid of a high and low fidelity problem containing 8 and 4 nodes respectively. The Δr_l values are selected such that the high and low temperature locations for the quantity of interest match.

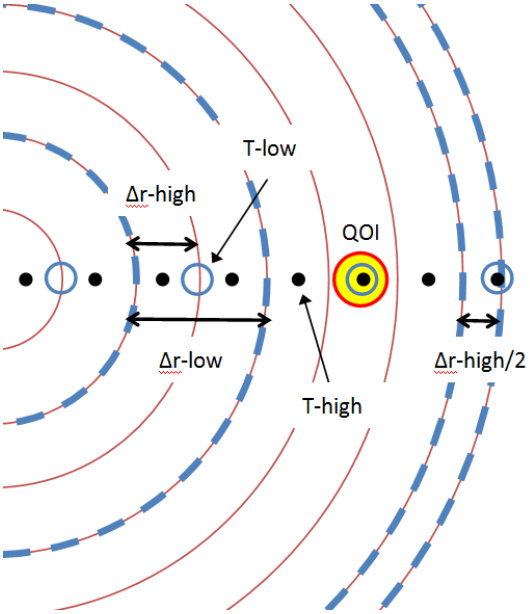

Figure 2.1: **Low and high fidelity representative mesh such that the quantity of interest locations match for four and eight ring models**

The adjusted parameters used in the low fidelity problem are defined as follows. For the fuel region, we have

$$k_{eff} = k_f \left[\frac{T_{f_{i+1,j}} - T_{f_{i,j}}}{\bar{T}_{f_{l+1,j}} - \bar{T}_{f_{l,j}}} \right] \frac{\Delta r_l}{\Delta r_i} \tag{2.4}$$

where the subscript l denotes the low fidelity node number and $\bar{T}_{f_{l,j}}$ denotes the high fidelity temperature solution mapped to the low fidelity mesh. Using k_{eff} values instead of k values ensures that the heat flux between radial rings is equal for both models.

Similarly, for the low fidelity coolant equations, the following adjusted convection coefficient is used

$$h_{eff} = h_c \left[\frac{T_{f_{N_r^*,j}} - T_{c_j}}{\bar{T}_{f_{N_{rl},j}} - \bar{T}_{c_{jl}}} \right] \tag{2.5}$$

where $\bar{T}_{f_{N_{rl},j}}$ and $\bar{T}_{c_{jl}}$ denote the low fidelity final ring temperature and coolant temperature respectively for node j. Similarly to the previous expression, this ensures that the heat flux at the pin boundary is the same for both the high and low fidelity. Using these adjusted parameters with the finite differenced coolant equations represented in the previous section will result in

an equality between high and low fidelity volume averaged temperatures. Because the adjusted parameters are calculated using steady state values, the average high fidelity fuel temperatures will not match the low fidelity fuel temperatures during transients.

Similarly to the high fidelity forward problem, the low fidelity steady state discretized problem is

$$\widetilde{\bar{\mathbf{A}}}\widetilde{\boldsymbol{\phi}} + \widetilde{\mathbf{d}} = 0 \tag{2.6}$$

with $\widetilde{\boldsymbol{\phi}} = \left[\widetilde{T_f}\ \widetilde{T_c}\right]^T$. The low fidelity steady state temperature operator $\widetilde{\bar{\mathbf{A}}}$ is a coarse version of $\bar{\bar{\mathbf{A}}}$ using the k_{eff} and h_{eff} constants for the fluid and fuel equations. The matrix structure of $\widetilde{\bar{\mathbf{A}}}$ will have the same structure as $\bar{\bar{\mathbf{A}}}$ but with fewer rows dedicated to radial temperatures.

The time dependent low fidelity solution will have the following structure

$$\widetilde{\bar{\mathbf{C}}}_{n+1}\widetilde{\boldsymbol{\phi}}_{n+1} = -\widetilde{\bar{\mathbf{B}}}_{n+1}\widetilde{\boldsymbol{\phi}}_n + \widetilde{\mathbf{Q}}_{n+1} \tag{2.7}$$

with

$$\begin{aligned}
\widetilde{\bar{\mathbf{C}}}_{n+1} &\equiv \left[\widetilde{\gamma}\bar{\bar{\mathbf{I}}} - \Delta t_n \widetilde{\bar{\mathbf{A}}}_{n+1}\right] \\
\widetilde{\bar{\mathbf{B}}}_{n+1} &\equiv \left[\widetilde{\gamma}\bar{\bar{\mathbf{I}}} - \Delta t_n \widetilde{\bar{\mathbf{A}}}_{n}\right] \\
\widetilde{\mathbf{Q}}_{n+1} &\equiv \alpha\Delta t_n \widetilde{\mathbf{d}}_{n+1} + (1-\alpha)\Delta t_n \widetilde{\mathbf{d}}_n
\end{aligned}$$

Linear interpolation between low fidelity temperatures for mapping onto the high fidelity mesh will also cause a discrepancy between fidelity temperatures for both steady state and time dependent problems. It is important to note that although the low fidelity problem is using a finite difference scheme on a coarser mesh, refinement is not the only difference between high fidelity and low fidelity problems. If this were the case, the adjoint methods presented in this thesis would simply be an extension to adaptive meshing applied to a heat conduction problem. Since the low fidelity problem uses adjusted convection and conduction coefficients in addition to linear interpolation, it can be thought of as a separate mathematical model for predicting fuel temperatures on a radial mesh comparable to the high fidelity finite difference scheme.

2.1.3 Forward Analytic Solution

An analytic solution to the steady state forward equations was determined for verification purposes. For this thesis, much of the verification work was done with the steady state problem

since time dependent adjoint behavior was found to be a trivial extension. A constant heat generation was assumed to help simplify analytic derivations. What follows is the determination of an analytic solution to the steady state forward problem with constant heat generation.

Start with the steady state forward problem definition

$$-\frac{k_f}{r}\frac{\partial}{\partial r}\left(r\frac{\partial T_f}{\partial r}\right) = q''' = \text{constant} \tag{2.8}$$

$$c_p^c \dot{m}_c \frac{dT_c}{dz} - 2\pi R q'' = 0 \tag{2.9}$$

$$T_c|_{z=0} = T_{c_{in}}, \quad \left.\frac{\partial T_f}{\partial r}\right|_{r=0} = 0$$

$$\left.-k_f \frac{\partial T_f}{\partial r}\right|_{r=R} = h_c\left(T_f|_{r=R} - T_c\right) = \left. q''\right|_{r=R}$$

Solving for the heat flux q'' at the pin surface:

$$q'''\left(\pi R^2 H\right) = q''\left(2\pi R H\right)$$

$$\left. q''\right|_{r=R} = q''' \frac{\pi R^2 H}{2\pi R H} = q''' \frac{R}{2}$$

The coolant equation becomes

$$\frac{\partial T_c}{\partial z} = q''' \frac{R}{2c_p^c \dot{m}_c} 2\pi R = \frac{q''' \pi R^2}{c_p^c \dot{m}_c}$$

Integrating from 0 to z

$$\int_0^z \left(\frac{\partial T_c}{\partial z'} = \frac{q''' \pi R^2}{c_p^c \dot{m}_c}\right) dz'$$

$$T_c(z) - T_c(0) = \frac{q''' \pi R^2}{c_p^c \dot{m}_c} z$$

$$T_c(z) = \frac{q''' \pi R^2}{c_p^c \dot{m}_c} z + T_c(0)$$

which is defined for a given incoming coolant temperature.

To solve for $T_f(r)$, the fuel equation is first integrated from 0 to r:

$$\int_0^r \left(-\frac{k_f}{r'}\frac{\partial}{\partial r'}\left(r'\frac{\partial T_f}{\partial r'}\right) = q'''\right) r' dr'$$

$$-k_f\, r' \frac{\partial T_f}{\partial r'}\bigg|_0^r = \frac{q'''}{2} r^2$$

Applying the boundary condition $\left.\frac{\partial T_f}{\partial r}\right|_{r=0} = 0$ results in

$$\frac{\partial T_f}{\partial r} = -\frac{q'''}{2k_f} r$$

Integrating from r to R

$$\int_r^R \left(\frac{\partial T_f}{\partial r'} = -\frac{q'''}{2k_f} r' \right) dr'$$

$$\left[T_f\left(r', z\right) = -\frac{q'''}{4k_f} r'^2 \right]_r^R$$

$$T_f(r,z) = T_f(R,z) + \frac{q'''}{4k_f}\left(R^2 - r^2\right)$$

Examining the boundary condition for $T_f(R)$:

$$q''\big|_{r=R} = q''' \frac{R}{2} = h_c \left(T_f(R,z) - T_c(z)\right)$$

$$T_f(R,z) = q''' \frac{R}{2h_c} + T_c(z)$$

and substituting this expression for $T_f(R,z)$ into the previous solution for $T_f(r,z)$ results in the following expression:

$$T_f(r,z) = q''' \frac{R}{2h_c} + T_c(z) + \frac{q'''}{4k_f}\left(R^2 - r^2\right)$$

This analytic forward solution is used for verification with the discrete forward problem as well as with the analytical adjoint.

2.2 Adjoint Problem

Adjoint techniques are employed in order to evaluate the difference between a high fidelity and low fidelity fuel temperature at specific locations of interest. In order to derive the functional, the following Quantity of Interest associated with the difference between the high and low fidelity solution is examined. This response is written as

$$\Re \equiv \left\langle \bar{f}_R, \bar{T} - \widetilde{T} \right\rangle_{t,z,r}$$

where subscripts t, z, and r define the dimensions of the inner product, $\bar{f}_R$ defines the response

function for the Quantity of Interest, $\bar{T}$ denotes the high-fidelity solution vector, and $\widetilde{T}$ denotes the low fidelity solution vector. The vector dependence captures the coolant and fuel temperatures, $\bar{T} = (T_f \; T_c)^T$. Set $\bar{Q}^\dagger \equiv \bar{f}_R$ and $\bar{\bar{A}}^\dagger \left[\bar{T}^\dagger\right] = \bar{Q}^\dagger$, where the matrix operators still denote continuous versus discretized operators, produces

$$\Re \equiv \left\langle \bar{f}_R, \bar{T} - \widetilde{T} \right\rangle_{t,z,r} = \left\langle \bar{\bar{A}}^\dagger[\bar{T}^\dagger], \bar{T} - \widetilde{T} \right\rangle_{t,z,r}$$
$$= \left\langle \bar{T}^\dagger, \bar{\bar{A}}[\bar{T} - \widetilde{T}] \right\rangle_{t,z,r} + BC + IC + FC = \left\langle \bar{T}^\dagger, \bar{\bar{A}}[\bar{T}] - \bar{\bar{A}}[\widetilde{T}] \right\rangle_{t,z,r} + BC + IC + FC$$

where BC, IC, and FC represent the boundary conditions, initial condition, and final condition that are the byproducts of the formulation of $\bar{\bar{A}}$ from $\bar{\bar{A}}^\dagger$. Note that the expression $\bar{\bar{A}}[\bar{T}] = \bar{Q}$ is exact. Therefore we have

$$\Re = \left\langle \bar{T}^\dagger, \bar{Q} - \bar{\bar{A}}[\widetilde{T}] \right\rangle + BC + IC + FC$$

After defining the residual, $\bar{r} = \bar{Q} - \bar{\bar{A}}[\widetilde{T}]$, the response is written as

$$\Re = \left\langle \bar{T}^\dagger, \bar{r} \right\rangle_{t,z,r} + BC + IC + FC$$

Properly defining the adjoint problem will ensure that

$$BC + IC + FC = 0$$

so that the only remaining term is the inner product. Therefore, given a residual from the low fidelity solution $\widetilde{T}$ operated on by the high fidelity operator, an inner product with the appropriate adjoint will yield the difference between the high and low fidelity temperatures at the appropriate location of interest.

This project investigated the possibility to estimate the response by using a low fidelity adjoint solution in place of the high fidelity adjoint. This approach would evaluate the response using

$$\widetilde{\Re} = \left\langle \widetilde{T}^\dagger, \bar{r} \right\rangle_{t,z,r}$$

where $\widetilde{T}^\dagger$ is the elongated low fidelity adjoint solution found by evaluating

$$\widetilde{\bar{\bar{A}}}^\dagger \left[\widehat{T}^\dagger\right] = \widetilde{Q}^\dagger$$

and

$$\widetilde{T}^{\dagger} = \widetilde{\bar{E}}_T^{\dagger} \hat{T}^{\dagger}$$

We define $\widetilde{\bar{E}}_t^{\dagger}$ is an elongation operator that projects the coarsened low fidelity adjoint solution onto the high fidelity mesh. This implies that if

$$\bar{\bar{A}}^{\dagger} \widetilde{\bar{E}}_T^{\dagger} \widetilde{\bar{A}}^{\dagger -1} = \widetilde{Q}^{\dagger} = \bar{Q}^{\dagger}$$

then exact values of the response are obtained. By inspection, it can be seen that if

$$\widetilde{\bar{E}}_T^{\dagger} \widetilde{\bar{A}}^{\dagger -1} = \bar{\bar{A}}^{\dagger -1}$$

holds, one would think that there may also be definitions for $\widetilde{Q}^{\dagger}$ that could enforce this equality. However, since $\widetilde{\bar{E}}_T^{\dagger}$ is a non-square matrix leading to an ill posed problem, the best one can do is a least squares approximation.

If the response found using the low fidelity adjoint solution results in temperature differences that are within an appropriate tolerance, then the low fidelity solution could be used to effectively estimate the difference between the high and low fidelity solutions without ever needing to explicitly solve the high fidelity problem. This method is the primary means for which a low fidelity problem can determine at which times and locations it is necessary to use a higher level of fidelity without unduly compromising its greater level of computational efficiency as compared to the high fidelity problem.

In order to accomplish this, an appropriate method for determining a low fidelity adjoint operator and elongation operator that will map the low fidelity problem onto the high fidelity spatial and temporal mesh must be developed. What follows in this section is a detailed account of various adjoint problem definitions and their resulting system of expressions used to determine either the high or the low fidelity adjoint solutions. Understanding their similarities and differences is integral to evaluating the behavior of adjoint methods used for adaptive model refinement.

2.2.1 Mathematical Adjoint

The mathematical adjoint is derived from the forward time dependent discretized problem much in the same way as described in section 1.3.2. Starting with the block matrix system from the discretized forward problem represented by equation (2.3)

$$\begin{bmatrix} \bar{\bar{\mathbf{C}}}_1 & & & \\ \bar{\bar{\mathbf{B}}}_2 & \bar{\bar{\mathbf{C}}}_2 & & \\ & \bar{\bar{\mathbf{B}}}_3 & \bar{\bar{\mathbf{C}}}_3 & \\ & & \ddots & \ddots \end{bmatrix} \begin{bmatrix} \bar{\phi}_1 \\ \bar{\phi}_2 \\ \bar{\phi}_3 \\ \vdots \end{bmatrix} = \begin{bmatrix} \bar{\mathbf{Q}}_1 \\ \bar{\mathbf{Q}}_2 \\ \bar{\mathbf{Q}}_3 \\ \vdots \end{bmatrix}$$

we derive the adjoint problem by taking the transpose of the above system.

$$\begin{bmatrix} \bar{\bar{\mathbf{C}}}_1^* & \bar{\bar{\mathbf{B}}}_2^* & & \\ & \bar{\bar{\mathbf{C}}}_2^* & \bar{\bar{\mathbf{B}}}_3^* & \\ & & \bar{\bar{\mathbf{C}}}_3^* & \ddots \\ & & & \ddots \end{bmatrix} \begin{bmatrix} \bar{\phi}_1^* \\ \bar{\phi}_2^* \\ \bar{\phi}_3^* \\ \vdots \end{bmatrix} = \begin{bmatrix} \bar{\mathbf{Q}}_1^* \\ \bar{\mathbf{Q}}_2^* \\ \bar{\mathbf{Q}}_3^* \\ \vdots \end{bmatrix}$$

with the adjoint matrix operators

$$\bar{\bar{\mathbf{C}}}^* = \bar{\bar{\mathbf{C}}}^{\mathbf{T}}, \qquad \bar{\bar{\mathbf{B}}}^* = \bar{\bar{\mathbf{B}}}^{\mathbf{T}}$$

and

$$\begin{aligned} \bar{\bar{\mathbf{C}}}_{n+1}^* &\equiv \left[\bar{\gamma}\bar{\bar{\mathbf{I}}} - \Delta t_n \bar{\bar{\mathbf{A}}}_{n+1}^*\right] \\ \bar{\bar{\mathbf{B}}}_{n+1}^* &\equiv \left[\bar{\gamma}\bar{\bar{\mathbf{I}}} - \Delta t_n \bar{\bar{\mathbf{A}}}_{n}^*\right] \\ \bar{\mathbf{Q}}_{n+1}^* &\equiv \alpha \Delta t_n \bar{\mathbf{d}}_{n+1}^* + (1-\alpha)\Delta t_n \bar{\mathbf{d}}_n^* \end{aligned}$$

This results in the general time dependent mathematical adjoint expression

$$\bar{\bar{\mathbf{C}}}_n^* \bar{\phi}_{n+1}^* + \bar{\bar{\mathbf{B}}}_{n+1}^* \bar{\phi}_n^* = \bar{\mathbf{Q}}_n^* \tag{2.10}$$

The matrix operator $\bar{\bar{\mathbf{A}}}_{n+1}^*$ is derived by taking the transpose of $\bar{\bar{\mathbf{A}}}_{n+1}$. Using the definition of this matrix shown previously, this transposed adjoint matrix becomes

$$\bar{\bar{\mathbf{A}}}^T = \begin{bmatrix} \bar{\bar{\mathbf{D}}}_f^T & \bar{\bar{\mathbf{O}}}_c^T \\ \bar{\bar{\mathbf{O}}}_f^T & \bar{\bar{\mathbf{D}}}_c^T \end{bmatrix}$$

with

$$\bar{\bar{\mathbf{D}}}_f^T = \begin{bmatrix} -a_2 & a_2 & & & & & \\ a_2 & b_3 & a_3 & & & & \\ & a_3 & b_4 & a_4 & & & \\ & & & \ddots & & & \\ & & & a_{N_r-2} & b_{N_r-1} & a_{Nr-1} & \\ & & & & a_{N_r-1} & e & \\ & & & & & \ddots & \end{bmatrix}, \quad \bar{\bar{\mathbf{O}}}_c^T = \begin{bmatrix} \vdots & & & & \\ f & & & & \\ & \ddots & & & \\ & & f & & \\ & & & \ddots & \\ & & & & f \end{bmatrix},$$

$$\bar{\bar{\mathbf{D}}}_c^T = \begin{bmatrix} m & k & & & \\ & m & k & & \\ & & & \ddots & \\ & & & & m \end{bmatrix}, \quad \bar{\bar{\mathbf{O}}}_f^T = \begin{bmatrix} \cdots & f & & \\ & & \ddots & \\ & & & f \end{bmatrix}$$

The definitions for the constants shown in the previous matrix are the same as those used for the forward matrix operator $\bar{\bar{\mathbf{A}}}_{n+1}$. Operating on the adjoint solution vector $\bar{\boldsymbol{\phi}}_n^* = \begin{bmatrix} \bar{T}_f^* & \bar{T}_c^* \end{bmatrix}^T$ results in a system of linear equations that can be solved with the given final condition $\bar{T}_f^* = \bar{T}_c^* = 0$.

Examination of Discrete Adjoint Equations as $\Delta r, \Delta z \to 0$

Multiplying the previously defined adjoint operator $\bar{\bar{A}}^*$ by it's solution vector $\bar{T}^* = \begin{bmatrix} T_f^* & T_c^* \end{bmatrix}^T$ results in the following set of equations.

$$a_{i-1}T^*_{f_{i-1,j}} + b_i T^*_{f_i,j} + a_i T^*_{f_{i+1,j}} = Q^*_{i,j} \qquad (1a)$$
$$a_{N_r-1}T^*_{f_{N_r-1,j}} + e{T^*_{f^*_{N_r,j}}}^* + fT^*_{c_j} = Q^*_{N_r,j} \qquad (2a)$$
$$fT^*_{f^*_{N_r,j}} + mT^*_{c_j} + hT^*_{c_{j+1}} = Q^*_{c_j} \qquad (3a)$$
$$fT^*_{f^*_{N_r^*,N_z}} + mT^*_{c_{N_z}} = Q^*_{c_{N_z}} \qquad (4a)$$

Examining equation $1a$, we have the following dicretized relationship

$$a_{i-1}T^*_{f_{i-1,j}} + b_i T^*_{f_i,j} + a_i T^*_{f_{i+1,j}}$$

$$= 2\pi k_f \frac{r_i}{\Delta r} T^*_{f_{i+1,j}} - 2\pi k_f \left(\frac{r_i}{\Delta r} + \frac{r_{i-1}}{\Delta r} \right) T^*_{f_i,j} + 2\pi k_f \frac{r_{i-1}}{\Delta r} T^*_{f_{i-1,j}}$$

$$= 2\pi k_f \left[r_i \frac{T^*_{f_{i+1,j}} - T^*_{f_i,j}}{\Delta r} - r_{i-1} \frac{T^*_{f_i,j} - T^*_{f_{i-1,j}}}{\Delta r} \right]$$

In order to examine this equation as it approaches the continuous or analytic adjoint equation, we operate on the previous expression with $\lim_{\Delta r \to 0}$

$$\lim_{\Delta r \to 0} \left(2\pi k_f \left[r_i \frac{T^*_{f_{i+1,j}} - T^*_{f_{i,j}}}{\Delta r} - r_{i-1} \frac{T^*_{f_{i,j}} - T^*_{f_{i-1,j}}}{\Delta r} \right] \right)$$

$$= 2\pi k_f \left[r \frac{\partial T^*_f}{\partial r} \right]_{r_i}^{r_{i+1}}$$

We then recognize that this expression is equal to

$$k_f \int_{r_i}^{r_{i+1}} dr 2\pi r \left[\frac{1}{r} \frac{\partial}{\partial r} \left(r \frac{\partial T^*_f}{\partial r} \right) \right] = k_f \int_{r_i}^{r_{i+1}} 2\pi r \nabla_r^2 T^*_f$$

Demanding point-wise equality of the energy balance equation implies the term

$$k_f \nabla_r^2 T^*_f$$

which matches the fuel temperature expression in the analytic adjoint.

Performing the same analysis on equation $2a$

$$a_{Nr-1} T^*_{f_{N_r-1,j}} + e T^*_{f^*_{N_r,j}} + f T^*_{c_j}$$

$$= 2\pi k_f \frac{r_{N_r-1}}{\Delta r} T^*_{f_{N_r-1,j}} - \left(2\pi k_f \frac{r_{N_r-1}}{\Delta r} + S_f h_c \right) T^*_{f^*_{N_r}} + 2\pi h_c T^*_{c_j}$$

$$= -2\pi k_f r_{N_r-1} \frac{T^*_{f^*_{N_r,j}} - T^*_{f_{N_r-1,j}}}{\Delta r} + 2\pi r_{N_r} h_c \left(T^*_{c_j} - T^*_{f^*_{N_r,j}} \right)$$

We then impose the following boundary condition

$$-k_f \left. \frac{\partial T^*_f}{\partial r} \right|_{r=R} = h_c \left(T^*_{f^*_{N_r,j}} - T^*_{c_j} \right)$$

resulting in

$$-2\pi k_f r_{N_r-1} \frac{T^*_{f^*_{N_r,j}} - T^*_{f_{N_r-1,j}}}{\Delta r} + 2\pi k_f \left. \frac{\partial T^*_f}{\partial r} \right|_{r=R}$$

We again operate on the previous expression with $\lim_{\Delta r \to 0}$

$$\lim_{\Delta r \to 0} 2\pi r_{N_r} k_f \left[\left. \frac{\partial T_f^*}{\partial r} \right|_{r=R} - r_{N_r - 1} \frac{T^*_{f_{N_r,j}} - T^*_{f_{N_r-1,j}}}{\Delta r} \right]$$

$$= 2\pi k_f \left[r \frac{\partial T_f^*}{\partial r} \right]_{r_{N_r-1}}^{r_{N_r}}$$

which results in

$$-2\pi k_f r_{N_r-1} \frac{T^*_{f_{N_r^*,j}} - T^*_{f_{N_r^*-1,j}}}{\Delta r} + 2_f \left. \frac{\partial T_f^*}{\partial r} \right|_{r=R}$$

Operate on the previous expression with $\lim_{\Delta r \to 0}$

$$\lim_{\Delta r \to 0} \left(-2\pi k_f r_{N_r-1} \frac{T^*_{f_{N_r^*,j}} - T^*_{f_{N_r^*-1,j}}}{\Delta r} + 2_f \left. \frac{\partial T_f^*}{\partial r} \right|_{r=R} \right)$$

$$= 2\pi k_f \left[r \frac{\partial T_f^*}{\partial r} \right]_{r_{N_r-1}}^{r_{N_r}}$$

Recognize that this expression is equal to

$$\int_{r_{N_r-1}}^{r_{N_r}} dr 2\pi r \left[\frac{1}{r} \frac{\partial}{\partial r} \left(r \frac{\partial T_f^*}{\partial r} \right) \right] = k_f \int_{r_{N_r-1}}^{r_{N_r}} dr 2\pi r \nabla_r^2 T_f^*$$

Again, demanding point wise equality of the energy balance term implies the term

$$= k_f \nabla_r^2 T_f^*$$

Examining equation $3a$ and noting that $S_f = 2\pi R$

$$f T^*_{f_{N_r^*,j}} + m T^*_{c_j} + h T^*_{c_{j+1}}$$

$$= S_f h_c T^*_{f_{N_r^*,j}} - \left(h_c S_f - \frac{c_{p_c} \dot{m}_c}{\Delta z} \right) T^*_{c_j} - \frac{c_{p_c} \dot{m}_c}{\Delta z} T^*_{c_{j+1}}$$

$$= -c_{p_c} \dot{m}_c \frac{T^*_{c_{j+1}} - T^*_{c_j}}{\Delta z} + h_c S_f \left(T^*_{f_{N_r^*,j+1}} - T^*_{c_j} \right)$$

We then impose the following source term

$$q''|_{r=R} = h_c \left(T^*_{f_{N_r^*,j}} - T^*_{c_j} \right)$$

Operate on the previous expression with $\lim_{\Delta z \to 0}$

$$\lim_{\Delta z \to 0} \left[-c_{p_c} \dot{m}_c \left(\frac{T^*_{c_{j+1}} - T^*_{c_j}}{\Delta z} \right) + S q'' \right]$$

$$= -c_{p_c} \dot{m}_c \frac{\partial T^*_c}{\partial z} + S \; q''|_{r=R}$$

Performing the limit analysis on equation $4a$

$$f T^*_{f_{N^*_r, N_z}} + m T^*_{c_{N_z}}$$

$$= S_f h_c T^*_{f_{N^*_r, N_z}} - \left(h_c S_f - \frac{c_{p_c} \dot{m}_c}{\Delta z} \right) T^*_{c_{N_z}}$$

$$= c_{pc} \dot{m}_c \left(\frac{T^*_{c_{N_z}}}{\Delta z} \right) + 2\pi R h_c \left(T^*_{f_{N_r, N_z}} - T^*_{c_{N_z}} \right)$$

It is inferred by the structure of the adjoint operator $\bar{\bar{A}}^\dagger$ shown previously that the following boundary conditions also apply:

$$\nabla \; T^\dagger_f \Big|_{r=0} = 0$$

$$T^\dagger_c \Big|_{z=H} = 0$$

From this analysis, we have the following adjoint equations

$$k_f \nabla^2 T^\dagger_f = Q^\dagger_f$$

$$c_{p_c} \dot{m}_c \frac{\partial T^\dagger_c}{\partial z} - \; q'' \big|_{r=R} = Q^\dagger_c$$

with the following boundary conditions

$$\nabla \; T^\dagger_f \Big|_{r=0} = 0 \qquad T^\dagger_c \Big|_{z=H} = 0$$

$$q''\big|^{\dagger}_{r=R} = h_c\left(T_f^{\dagger}\Big|_{r=R} - T_c^{\dagger}\right) = -k_f\left.\frac{\partial T_f^{\dagger}}{\partial r}\right|_{r=R}$$

2.2.2 Analytic Adjoint

An alternative way to derive the adjoint equations is to consider an adjoint problem as derived from the continuous forward equations. This process is briefly described in section 1.3.2 and is now presented in detail for the time dependent forward equations. For this derivation, it was necessary to derive a functional based on the forward operators. Rewrite the forward analytic equations (1.5) - (1.9) as operators on temperature values

$$O_c(\ ) \equiv c_p^c \rho_c A_x \frac{\partial(\ )}{\partial t} + c_p^c \dot{m}_c \frac{\partial(\ )}{\partial z}$$
$$O_f(\ ) \equiv c_p^f \rho_f \frac{\partial(\ )}{\partial t} - k_f \nabla_r^2(\ )$$

$$O_c\left[T_c\right] = -S_f k_f \nabla_r\ T_f|_{r=R}$$
$$O_f\left[T_f\right] = q'''$$

$$h\left(T_f|_{r=R} - T_c\right) = -k_f \nabla_r\ T_f|_{r=R}$$
$$T_c|_{t=0} = T_c^{(o)} \qquad T_c|_{z=0} = T_c^{In}$$
$$T_f|_{t=0} = T_f^{(o)} \qquad \nabla_r\ T_f|_{r=o} = 0$$

The Quantity of Interest associated with the difference between the high fidelity solution and the low fidelity solution is examined. This response is written as

$$\Re \equiv \left\langle \bar{f}_R, \bar{T} - \widetilde{T} \right\rangle_{t,z,r} = \left\langle \bar{T}^{\dagger}, \bar{Q} - \bar{\bar{A}}[\widetilde{T}] \right\rangle + BC + IC + FC$$

After defining the residual, $\bar{r} = \bar{Q} - \bar{\bar{A}}[\widetilde{T}]$, the following expression is produced:

$$\Re = \left\langle \bar{T}^{\dagger}, \bar{r} \right\rangle_{t,z,r} + BC + IC + FC$$

Writing out the forward equations reveals the action of the $\bar{\bar{A}}$ operator for which we seek the adjoint and associated BC, IC, and FC terms. We also scale the coolant equation by $\left[\frac{R^2}{2}\frac{S_f}{R}\right]^{-1} = \left[\frac{1}{\pi R^2}\right]$ anticipating the necessity to relate the fuel and coolant terms with one another. The fuel and coolant equations are then.

$$\left[\tfrac{1}{\pi R^2}\right]\left(c_p^c\rho_c A_x\tfrac{\partial}{\partial t}+c_p^c\dot{m}_c\tfrac{\partial}{\partial z}\right)T_c+\left[\tfrac{1}{\pi R^2}\right]\left(k_f S_f\nabla_r T_f|_R\right)=0$$

$$\left(c_p^f\rho_f\tfrac{\partial}{\partial t}-k_f\nabla_r^2\right)T_f=q'''$$

By demanding that

$$\left\langle\bar{T}^\dagger,\bar{\bar{A}}\bar{T}\right\rangle=\left\langle\bar{\bar{A}}^\dagger\bar{T}^\dagger,\bar{T}\right\rangle$$

for any $\bar{T}$ and $\bar{T}^\dagger$ that satisfies specified BC, IC, and FC, the equations are defined along with the BC, IC, and FC terms. Demanding this holds for any $\bar{T}$ and $\bar{T}^\dagger$ implies point-wise enforcement. The forward equations and their respective boundary and initial conditions are known. To obtain the similar equations for the adjoint problem, the operator must be isolated to operate on the adjoint temperatures in the inner products. The required equations are found by writing the inner products and using integration by parts.

$$\left\langle T_c^\dagger,\left[\tfrac{1}{\pi R^2}\right]c_p^c\rho_c A_x\tfrac{\partial T_c}{\partial t}\right\rangle_{t,z,r}=\left[\tfrac{1}{\pi R^2}\right]c_p^c\rho_c A_x\int_0^R rdr\int_0^H dz\int_0^{t_F}dt\tfrac{\partial T_c}{\partial t}T_c^\dagger$$

$$=\left[\tfrac{1}{\pi R^2}\right]c_p^c\rho_c A_x\int_0^R rdr\int_0^H dz\left[T_c^\dagger T_c\Big|_0^{t_f}-\int_0^{t_F}dt\tfrac{\partial T_c^\dagger}{\partial t}T_c\right]$$

$$=\left[\tfrac{1}{\pi R^2}\right]c_p^c\rho_c A_x\left\langle T_c^\dagger,T_c\right\rangle_{z,r}\Big|_0^{t_F}-\left[\tfrac{1}{\pi R^2}\right]c_p^c\rho_c A_x\left\langle\tfrac{\partial T_c^\dagger}{\partial t},T_c\right\rangle_{t,z,r}$$

The $\left\langle c_p^f\rho_f T_f^\dagger,\frac{\partial T_f}{\partial t}\right\rangle$ and $\left\langle T_c^\dagger,\left[\frac{1}{\pi R^2}\right]c_p^c\dot{m}_c\frac{\partial T_c}{\partial z}\right\rangle$ inner products are developed similarly such that

$$\left\langle T_f^\dagger,c_p^f\rho_f\tfrac{\partial T_f}{\partial t}\right\rangle_{t,z,r}=c_p^f\rho_f\left\langle T_f^\dagger,T_f\right\rangle_{z,r}\Big|_0^{t_F}-c_p^f\rho_f\left\langle\tfrac{\partial T_f^\dagger}{\partial t},T_f\right\rangle_{t,z,r}$$

$$\left\langle T_c^\dagger,\left[\tfrac{1}{\pi R^2}\right]c_p^c\dot{m}_c\tfrac{\partial T_c}{\partial z}\right\rangle_{t,z,r}=\left[\tfrac{1}{\pi R^2}\right]c_p^c\dot{m}_c\left\langle T_c^\dagger,T_c\right\rangle_{t,r}\Big|_0^H-\left[\tfrac{1}{\pi R^2}\right]c_p^c\dot{m}_c\left\langle\tfrac{\partial T_c^\dagger}{\partial z},T_c\right\rangle_{t,z,r}$$

Green's Theorem is applied to $\left\langle T_f^\dagger,-k_f\nabla_r^2T_f\right\rangle$ to obtain

$$\left\langle T_f^\dagger,-k_f\nabla_r^2T_f\right\rangle_{t,z,r}=-k_f\left\langle T_f^\dagger,r\nabla_r T_f-T_f,r\nabla_r T_f^\dagger\right\rangle_{t,z}\Big|_0^R-k_f\left\langle\nabla_r^2T_f^\dagger,T_f\right\rangle_{t,z,r}$$

The resulting BC, IC, and FC terms found in the functional are

$$\left\langle T_c^\dagger, \left[\tfrac{1}{\pi R^2}\right] c_p^c \rho_c T_c \right\rangle_{z,r}\Big|_0^{t_F}, \quad \left\langle T_f^\dagger, c_p^f \rho_f T_f \right\rangle_{z,r}\Big|_0^{t_F}, \quad \left\langle T_c^\dagger, \left[\tfrac{1}{\pi R^2}\right] c_p^c \dot{m}_c T_c \right\rangle_{t,r}\Big|_0^{H},$$
$$-k_f \left\langle T_f^\dagger, r\nabla_r T_f - T_f, r\nabla_r T_f^\dagger \right\rangle_{t,z}\Big|_0^{R}$$

Included in this list of remaining terms is the inner product with $T_c^\dagger$ with the following heat flux term from the coolant equation

$$\left\langle T_c^\dagger, \left[\tfrac{1}{\pi R^2}\right] k_f S_f \nabla_r T_f\big|_R \right\rangle_{t,z,r}$$

Noting that T_c and T_f actually denote $\Delta T_c \equiv T_c - T_c^{(o)}$ and $\Delta T_f \equiv T_f - T_f^{(o)}$, the "natural" boundary and initial conditions for the forward problem are imposed. These conditions are written as

$$T_c|_{z=0} = T_c|_{t=0} = T_f|_{t=0} = 0$$

Additionally, the adjoint final and boundary conditions are free to select and imposed to be the following to remove the BC and FC terms

$$T_c^\dagger\Big|_{z=H} = T_c^\dagger\Big|_{t=t_F} = T_f^\dagger\Big|_{t=t_F} = 0$$

The remaining terms that appear in the functional are as follows:

$$-k_f \left\langle T_f^\dagger, r\nabla_r T_f - T_f, r\nabla_r T_f^\dagger \right\rangle_{t,z}\Big|_0^{R} + \left\langle T_c^\dagger, \left[\tfrac{1}{\pi R^2}\right] k_f S_f \nabla_r T_f\big|_R \right\rangle_{t,z,r}$$

The expression $\left\langle T_f^\dagger, r\nabla_r T_f - T_f, r\nabla_r T_f^\dagger \right\rangle_{t,z}\Big|_{r=0} = 0$ is true due both to symmetry within the geometry of the problem as well as due to the r variable present. The remaining terms

$$-k_f R \left\langle T_f^\dagger, \nabla_r T_f - T_f, \nabla_r T_f^\dagger \right\rangle_{t,z}\Big|_{r=R} + \left\langle T_c^\dagger, \left[\tfrac{1}{\pi R^2}\right] k_f S_f \nabla_r T_f\big|_R \right\rangle_{t,z,r}$$

can be eliminated by first completing the r integration of the second term. This is possible since there is no r dependence of the function's inner product. This produces

$$\left(\tfrac{R^2}{2}\right) \left[\tfrac{1}{\pi R^2}\right] S_f k_f \left\langle T_c^\dagger, \nabla_r T_f \right\rangle_{t,z}\Big|_{r=R} = k_f R \left\langle T_c^\dagger, \nabla_r T_f \right\rangle_{t,z}\Big|_{r=R}$$

This will produce the remaining BC terms in the functional

$$-k_f R \left\langle T_f^\dagger, \nabla_r T_f - T_f, \nabla_r T_f^\dagger \right\rangle_{t,z}\Big|_{r=R} + k_f R \left\langle T_c^\dagger, \nabla_r T_f \right\rangle_{t,z}\Big|_R = 0$$

Next we impose

$$-k_f \nabla_r T_f|_{r=R} = h_c \left(T_f|_{r=R} - T_c \right)$$

which produces the following BC terms in the functional

$$h_c R \left\langle T_f^\dagger, (T_f - T_c) \right\rangle\Big|_{r=R} + k_f R \left\langle T_f, \nabla_r T_f^\dagger \right\rangle_{t,z}\Big|_{r=R} - h_c R \left\langle T_c^\dagger, (T_f - T_c) \right\rangle_{t,z}\Big|_{r=R}$$

$$= R \left\langle T_f, \left[k_f \nabla_r T_f^\dagger + h_c \left(T_f^\dagger - T_c^\dagger \right) \right] \right\rangle_{t,z}\Big|_{r=R} - h_c R \left\langle T_c, \left(T_f^\dagger - T_c^\dagger \right) \right\rangle_{t,z}\Big|_{r=R}$$

To make stationary with respect to T_f, impose

$$-k_f \nabla_r T_f^\dagger\Big|_{r=R} = h_c \left(T_f^\dagger\Big|_{r=R} - T_c^\dagger \right)$$

which eliminates the first term in the remaining functional. For the final term, we use the previously defined BC and return the r dependence to the inner product.

$$-h_c R \left\langle T_c, \left(T_f^\dagger - T_c^\dagger \right) \right\rangle_{t,z}\Big|_{r=R} = \left\langle T_c, \tfrac{2}{R} k_f \, \nabla_r T_f^\dagger\Big|_{r=R} \right\rangle_{t,z,r}$$

Let us define the adjoint heat flux at the pin surface as:

$$q''^\dagger\Big|_{r=R} = -k_f \nabla_r T_f^\dagger\Big|_{r=R} = h_c \left(T_f^\dagger\Big|_{r=R} - T_c^\dagger \right)$$

Gathering up all terms with T_c on one side of the inner product produces the following:

$$\tfrac{-1}{\pi R^2} \left[c_p^c \rho_c A_c \tfrac{\partial(\,)}{\partial t} + c_p^c \dot{m}_c \tfrac{\partial(\,)}{\partial z} \right] T_c^\dagger - \tfrac{2}{R} \, q''^\dagger\Big|_{r=R} = Q_c^\dagger$$

which can be scaled similarly to the forward coolant equation by multiplying through by πR^2.

Doing likewise for T_f produces

$$-\left[c_p^f \rho_f \tfrac{\partial(\,)}{\partial t} + k_f \nabla_r^2(\,) \right] T_f^\dagger = Q_f^\dagger$$

Summarizing the following analytic adjoint operators and previously defined boundary conditions are given by

$$O_c^\dagger(\ ) = -c_p^c \rho_c A_c \frac{\partial(\ )}{\partial t} - c_p^c \dot{m}_c \frac{\partial(\ )}{\partial z}$$
$$O_f^\dagger(\ ) = -\rho_f \frac{\partial(\ )}{\partial t} - k_f \nabla_r^2(\ )$$

$$O_c^\dagger \left[T_c^\dagger\right] = -S_f k_f \nabla_r\, T_f^\dagger\Big|_{r=R} + Q_c^\dagger$$
$$O_f^\dagger \left[T_f^\dagger\right] = Q_f^\dagger$$

F.C. $$T_c^\dagger\Big|_{t=t_F} = \quad T_f^\dagger\Big|_{t=t_F} = 0$$

B.C. $$T_c^\dagger\Big|_{z=H} = 0, \quad \nabla_r\, T_f^\dagger\Big|_{r=0} = 0$$
$$-k_f \nabla_r T_f^\dagger\Big|_{r=R} = h_c \left(T_f^\dagger\Big|_{r=R} - T_c^\dagger\right) = q''^\dagger\Big|_{r=R}$$

These equations are equivalent to the previously presented adjoint equations (1.10) - (1.14). In order to solve these equations, a similar discretization technique to that of the forward high fidelity solution is employed.

2.2.3 Analytic Adjoint Solution

An analytic solution to the adjoint equations was derived in order to help verify mathematical and physical adjoint behavior. Similar to the analytical solution derived for the forward problem, the system is assumed to be at steady state. These steady state adjoint equations as determined by the analytic adjoint problem derivation can be written as

$$-\frac{k_f}{r}\frac{\partial}{\partial r}\left(r\frac{\partial T_f^*}{\partial r}\right) = Q^* \tag{2.11}$$

$$-c_p^c \dot{m}_c \frac{dT_c^*}{dz} - 2\pi R q''^* = 0 \tag{2.12}$$

$$T_c^*|_{z=H} = 0, \quad \frac{\partial T_f^*}{\partial r}\Big|_{r=0} = 0$$

$$-k_f \frac{\partial T_f^*}{\partial r}\Big|_{r=R} = h_c \left(T_f^*|_{r=R} - T_c^*\right) = q''^*|_{r=R}$$

The adjoint source term is defined at the location of interest as

$$Q^* = \frac{1}{2\pi r}\delta\left(r - r_o\right)\delta\left(z - z_o\right)$$

We first examine the problem space for $z_o < z \leq H$. Integrating equation (2.11) from $r' = (0, r)$ with $0 \leq r < R$ and applying the boundary condition at $r = 0$ results in the

following expression for T_f^*:

$$\int_0^r dr' 2\pi r' \left[\frac{-k_f}{r'} \frac{\partial}{\partial r} \left(r' \frac{\partial T_f^*}{\partial r'} \right) = 0 \right]$$

$$r' \frac{\partial T_f^*}{\partial r'} \Big|_0^r = r \frac{\partial T_f^*}{\partial r} = 0$$

$$T_f^*(r,z) = \text{constant in r}$$

Therefore, $q''^*|_{r=R} = -k_f \frac{\partial T_f^*}{\partial r}_{r=R} = 0$ for $z_o < z \leq H$. Integrating equation (2.12) from $z' = (z, H)$ with $z_o < z \leq H$ and applying the boundary condition at $z = H$ results in the following expression for T_c^*:

$$\int_z^H dz' \left[-c_p^c \dot{m}_c \frac{dT_c^*}{dz'} \right] = 0$$

$$T_c^*|_z^H = \text{constant}$$

$$T_c^* = 0$$

In order to satisfy the boundary condition at $r = R$, it follows that $T_f^* \Big|_{r=R} = T_c^*$ and thus $T_f^* = 0$ for $z_o < z \leq H$ and all r.

Consider the analytical solution at $z = z_o$. By the previous argument, the adjoint fuel temperature solution for $0 \leq r < r_o$ and $z = z_o$ is

$$T_f^*(r,z)\big|_{z=z_o} = c_o \, f_o(z)|_{z=z_o}$$

where $f_o(z)$ is some function of z. Considering the limit of the solution a distance of $\epsilon << 1$ around r_o, a boundary condition at the $r = r_o$ and $z = z_o$ position is

$$\lim_{\epsilon \to 0} \left[\int_{r_o-\epsilon}^{r_o+\epsilon} -2\pi r dr \frac{k_f}{r} \frac{\partial}{\partial r} \left(r \frac{\partial T_f^*}{\partial r} \right) = \int_{r_o-\epsilon}^{r_o+\epsilon} 2\pi r dr \frac{\delta(r - r_o)\,\delta(z - z_o)}{2\pi r} \right]_{z=z_o}$$

$$\lim_{\epsilon \to 0} \left[-k_f (2\pi r) \, \frac{\partial T_f^*}{\partial r} \Big|_{r_o-\epsilon}^{r_o+\epsilon} = \delta(z - z_o) \right]_{z=z_o}$$

This implies that

$$T_f^*(r,z) = \hat{T}_f^*(r) \delta(z - z_o)$$

Dividing through by $\delta(z - z_o)$ results in the following expression

$$\lim_{\epsilon\to 0}\left[-k_f\left(2\pi r\right)\left.\frac{\partial\hat{T}_f^*}{\partial r}\right|_{r_o-\epsilon}^{r_o+\epsilon}=1\right]_{z=z_o}$$

Noting that $\hat{T}_f^*(r)=c_o$ for $r<r_0$, we can eliminate the derivative at $r_o-\epsilon$ and are left with

$$\lim_{\epsilon\to 0}\left[-k_f\left(2\pi r\right)\left.\frac{\partial\hat{T}_f^*}{\partial r}\right|_{r_o+\epsilon}=1\right]_{z=z_o}$$

which defines a boundary condition.

Integrating the fuel adjoint equation from $r_o+\epsilon$ to r for $r_o<r\leq R$ and using the previously defined boundary condition results in the following:

$$\lim_{\epsilon\to 0}\left[\int_{r_o+\epsilon}^{r}\left(-\frac{k_f}{r'}\frac{\partial}{\partial r'}\left(r'\frac{\partial T_f^*}{\partial r'}\right)\right)2\pi r'dr'\right]_{z=z_o}=0$$

$$\lim_{\epsilon\to 0}\left[-2\pi k_f r'\left.\frac{\partial T_f^*}{\partial r'}\right|_{r_o+\epsilon}^{r}\right]_{z=z_o}=0$$

$$\left.-2\pi k_f r\frac{\partial T_f^*}{\partial r}-1\right|_{z=z_o}=0$$

$$\left.\frac{\partial T_f^*}{\partial r}\right|_{z=z_o}=\frac{1}{r}\left(\frac{-1}{2\pi k_f}\right)$$

which satisfies the BC at $r_o+\epsilon$. The general solution for the above differential equation is

$$\left.T_f^*\right|_{z=z_o}=\left(\tilde{c}_o+\tilde{c}_1\ln r\right)\left.f_1(z)\right|_{z=z_o}$$

with

$$\tilde{c}_1=-\frac{1}{2\pi k_f}$$

The temperature across the interface at r_o is constrained such that

$$\lim_{\epsilon\to 0}\left[T_f^*\left(r_o+\epsilon\,,z\right)=T_f^*\left(r_o-\epsilon,z\right)\right]_{z=z_o}$$

This can be justified due to the fact that integrating the Q^* delta function across r_o at $z=z_o$ produces an expression for the derivative of $\left.T_f^*\right|_{z=z_o}$ that is finite. Since the derivative of $\left.T_f^*\right|_{z=z_o}$ at $r=r_o$ is finite, there can be no jump discontinuity in $\left.T_f^*\right|_{z=z_o}$ at $r=r_o$ and the

previously defined constraint holds. This implies that

$$[f_o(z) = f_1(z) = \delta(z - z_o)]_{z=z_o}$$

Applying the boundary condition for $T_f^*\Big|_{z=z_o}$ at $r = r_o + \epsilon$ results in the following expression for c_o

$$c_o = \frac{-1}{2\pi k_f} \ln r_o + \tilde{c}_o$$

Substituting $T_f^* = \tilde{c}_o + \tilde{c}_1 \ln(r)$ into the pin surface boundary condition at $r = R$ and integrating in the limit about z_o results in the following pin surface relationship

$$-k_f \frac{\tilde{c}_1}{R} = h \left(\tilde{c}_1 \ln R + \tilde{c}_o - \lim_{\epsilon \to 0} \int_{z_o - \epsilon}^{z_o + \epsilon} T_c^*(z) dz \right)$$

The term $\int_{z_o-\epsilon}^{z_o+\epsilon} T_c^*(z)dz = 0$ due to the fact that $T_c^*(z)$ is finite over the interval. Solving for $\tilde{c}_o$

$$\begin{aligned} \tilde{c}_o &= \left(\frac{k_f}{hR} + \ln R \right) \left(\frac{-1}{2\pi k_f} \right) \\ &= \frac{1}{2\pi} \left(\frac{1}{hR} + \frac{1}{k_f} \ln R \right) \end{aligned}$$

Integrating about $z = z_o$ in the limit, the adjoint coolant equation is written as

$$\lim_{\epsilon \to 0} \int_{z_o - \epsilon}^{z_o + \epsilon} \left[-c_p^c \dot{m}_c \frac{dT_c^*(z)}{dz} = 2\pi R q''^* = -2\pi R \frac{1}{2\pi k_f} \frac{k_f}{R} \delta(z - z_o) = \delta(z - z_o) \right]$$

producing

$$\lim_{\epsilon \to 0} T_c^*(z) \Big|_{z-\epsilon}^{z+\epsilon} = -\frac{1}{c_p^c \dot{m}_c}$$

Using the solution for $z > z_o$ renders

$$\lim_{\epsilon \to 0} T_c^*(z - \epsilon) = \frac{1}{c_p^c \dot{m}_c}$$

which is a jump boundary condition for T_c^* at $z = z_o$.

Solving the adjoint coolant equation for $0 \leq z < z_o$ obtains $T_c^*(z) = \tilde{c}_3$, therefore we have for $0 \leq z < z_o$

$$T_c^*(z) = \tilde{c}_3 = \lim_{\epsilon \to 0} T_c^*\left(z_o - \epsilon\right) = \frac{1}{c_p^c \dot{m}_c}$$

As shown for $z > z_o$, there is a solution for the adjoint fuel temperature with $z < z_o$ such that

$$T_f^*\left(r, z\right) = \text{constant in r}$$

Applying the boundary condition and solving for $T_f^*(r, z)$ with $z < z_o$,

$$-k_f \frac{\partial T_f^*}{\partial r}\bigg|_{r=R} = 0 = h_c \left(T_f^*\big|_{r=R} - T_c^* \right)$$

$$T_f^*\left(r, z\right) = T_f^*\big|_{r=R} = \frac{1}{c_p^c \dot{m}_c}$$

Thus the analytical solution for the adjoint coolant and fuel temperatures for a location of interest at $z = z_o$ and $r = r_o$ can be written as

$$T_f^*(r,z) = \begin{cases} 0 & 0 \le r \le R, \quad z_o < z \le H \\ c_o \delta(z - z_o) & 0 \le r < r_o, \quad z = z_o \\ \left(c_o + \tilde{c}_1 \ln\left(\dfrac{r}{r_o}\right) \right) \delta\left(z - z_o\right) & r_o \le r \le R, \quad z = z_o \\ c_1 & 0 \le r \le R, \quad 0 \le z < z_o \end{cases}$$

$$T_c^*(z) = \begin{cases} 0 & z_o < z \le H \\ c_1 & 0 \le z < z_o \end{cases}$$

with

$$\begin{aligned} c_o &= \frac{1}{2\pi}\left(\frac{1}{hR} + \frac{1}{k_f} \ln\left(\frac{R}{r_o}\right) \right) \\ c_1 &= \frac{1}{c_p^c \dot{m}_c} \\ \tilde{c}_1 &= -\frac{1}{2\pi k_f} \end{aligned}$$

This analytic solution only applies to steady state systems with the Q^* defined by Dirac delta functions as noted. In order to analyze the discrete system, we have to change the definition of Q^* to match the discrete adjoint source term.

Physical Error Metric for High and Low Fidelity Solutions

For verification of the physical high fidelity solution, the response function $\Re \equiv \left\langle \bar{f}_R, \bar{T} - \widetilde{\bar{T}} \right\rangle_{z,r}$ is evaluated using the analytic solutions to the steady state adjoint and forward problems. The low fidelity solution is defined to be a constant in both the fuel and coolant regions of the problem space and is written as:

$$\widetilde{T}_f(r,z) = \widetilde{T}_c(z) = b_0$$

This low fidelity analytical solution will hold for the initial condition and all forward boundary conditions if $b_o = T_c(z)|_{z=0}$.

In order to evaluate the error metric, the residual $\bar{r} = A[\widetilde{T}] - Q$ is determined using the previously defined low fidelity solution:

$$-\frac{k_f}{r}\frac{\partial}{\partial r}\left(r\frac{\partial}{\partial r}\left(\widetilde{T}_f\right)\right) - q''' = -\frac{k_f}{r}\frac{\partial}{\partial r}\left(r\frac{\partial}{\partial r}\left(b_o\right)\right) - q'''$$
$$= -q'''$$

$$c_p^c \dot{m}_c \frac{d}{dz}\left(\widetilde{T}_c\right) + 2\pi R k_f \left.\frac{\partial \widetilde{T}_f}{\partial r}\right|_{r=R} = c_p^c \dot{m}_c \frac{d}{dz}\left(b_o\right) - 2\pi R k_f \frac{\partial}{\partial r}\left(b_o\right)$$
$$= 0$$

The residual vector for the given low fidelity $\widetilde{T}$ solution is therefore

$$\bar{r} = \begin{bmatrix} -q''' & 0 \end{bmatrix}^T$$

The inner product $\left\langle \bar{T}^*, \bar{r} \right\rangle_{z,r}$ should be equal to $\left\langle \bar{Q}^*, \bar{e} \right\rangle_{z,r} = e(r_o, z_o)$. This error term can be written explicitly as

$$e(r_o, z_o) = b_o - T_f(r_o, z_o)$$
$$= -q''' \frac{R}{2h_c} - \frac{q'''}{4k_f}\left(R^2 - r_o^2\right) - \frac{q'''\pi R^2 z_o}{c_p^c \dot{m}_c} - T_c(0) + b_o$$

Rewriting $T_f^*(r,z)$ using heaviside step functions

$$T_f^*(r,z) = \left[1 - H\left(z - z_o\right)\right] c_1 + c_o \delta\left(z - z_o\right) + H\left(r - r_o\right) \tilde{c}_1 \ln\left(\frac{r}{r_o}\right) \delta\left(z - z_o\right)$$

evaluating the inner product $\left\langle \bar{T}^*, \bar{r} \right\rangle_{z,r}$

$$\left\langle \bar{T}^*, \bar{r} \right\rangle_{z,r} = \int_0^R 2\pi r dr \int_0^H dz \left[-q''' \left(T_f^*(r,z) \right] \right.$$

$$= -2\pi q''' \left[\int_0^R r dr \int_0^{z_o} dz \; c_1 + \int_0^R r dr \; c_o + \int_{r_o}^R r dr \tilde{c}_1 \ln\left(\frac{r}{r_o}\right) \right]$$

$$= -2\pi q''' \left[\frac{R^2 z_o c_1}{2} + \frac{c_o}{2} R^2 - \frac{\tilde{c}_1}{2} \ln r_o \left(R^2 - r_o^2 \right) + \frac{\tilde{c}_1}{4} \left[R^2 \left(2 \ln R - 1 \right) - r_o^2 \left(2 \ln r_o - 1 \right) \right] \right]$$

Rewriting using the definition of the constants from the analytical adjoint derivation

$$= -2\pi q''' \left[\frac{R^2 z_o}{2 c_p^c \dot{m}_c} - \frac{r_o^2}{4\pi k_f} \ln r_o + \frac{R^2}{2} \left[\frac{1}{2\pi} \left(\frac{1}{h_c R} + \frac{1}{k_f} \ln R \right) \right] \right.$$
$$\left. - \frac{1}{8\pi k_f} \left[R^2 \left(2 \ln R - 1 \right) - r_o^2 \left(2 \ln r_o - 1 \right) \right] \right]$$

$$= -2\pi q''' \left[\frac{R^2 z_o}{2 c_p^c \dot{m}_c} - \cancel{\frac{r_o^2}{4\pi k_f} \ln r_o} + \frac{R}{4\pi h_c} + \cancel{\frac{R^2}{4\pi k_f} \ln R} \right.$$
$$\left. - \cancel{\frac{R^2}{4\pi k_f} \ln R} + \frac{R^2}{8\pi k_f} + \cancel{\frac{r_o^2}{4\pi k_f} \ln r_o} - \frac{r_o^2}{8\pi k_f} \right]$$

$$= -2\pi q''' \left[\frac{R^2 z_o}{2 c_p^c \dot{m}_c} + \frac{R}{4\pi h_c} + \frac{1}{8\pi k_f} \left(R^2 - r_o^2 \right) \right]$$

$$= -\frac{q''' \pi R^2 z_o}{c_p^c \dot{m}_c} - \frac{q''' R}{h_c} - \frac{q'''}{4 k_f} \left(R^2 - r_o^2 \right)$$

setting $b_o = T_c(0)$, we have

$$\left\langle \bar{T}^*, \bar{r} \right\rangle_{z,r} = -\frac{q''' \pi R^2 z_o}{c_p^c \dot{m}_c} - \frac{q''' R}{h_c} - \frac{q'''}{4 k_f} \left(R^2 - r_o^2 \right) = \left\langle \bar{Q}^*, \bar{e} \right\rangle_{z,r}$$

which shows that the analytical adjoint solution in conjunction with the analytic forward solution can exactly calculate the difference between the high and low fidelities at a given location of interest.

Analytic Adjoint Solution Using Discrete Step Function for Q*

In order to apply the analytical adjoint solution to the discretized mathematical problem, a Q^* value was needed that matched the discretized $\bar{Q}^*$ used by the mathematical adjoint. We reconsider the analytic adjoint solution as a Green's Function for a source at r_o, z_o that produces a response at r, z. The analytic adjoint equations are then denoted as follows

$$O_f^*\left(T_f^*\right) = Q_{f,p}^*(r_o, z_o)$$

$$O_c^*\left(T_c^*\right) = 0$$

resulting in the following solution for $T_f^*(r_o, z_o \to r, z)$ and $T_c^*(z_o \to z)$

$$T_f^*(r_o, z_o \to r, z) = \begin{cases} 0 & 0 \le r \le R, \quad z_o < z \le H \\ c_o \delta(z - z_o) & 0 \le r < r_o, \quad z = z_o \\ \left(c_o + \tilde{c}_1 \ln\left(\dfrac{r}{r_o}\right)\right) \delta\left(z - z_o\right) & r_o \le r \le R, \quad z = z_o \\ c_1 & 0 \le r \le R, \quad 0 \le z < z_o \end{cases}$$

$$T_c^*(z_o \to z) = \begin{cases} 0 & z_o < z \le H \\ c_1 & 0 \le z < z_o \end{cases}$$

with

$$\begin{aligned} c_o &= \frac{1}{2\pi}\left(\frac{1}{hR} + \frac{1}{k_f}\ln\left(\frac{R}{r_o}\right)\right) \\ c_1 &= \frac{1}{c_p^c \dot{m}_c} \\ \tilde{c}_1 &= -\frac{1}{2\pi k_f} \end{aligned}$$

Noting that this is a Green's function or solution to the adjoint equations with a unit point source $Q_{f,p}^*(r_o, z_o)$, it is possible to determine an analytical solution using a step function source condition synonymous to the one used by the mathematical adjoint problem using the appropriate convolution. By definition, the discrete mathematical adjoint source is a step function between two discretized radial and axial node locations that are equidistant to a location of interest. This step source can be written as

$$Q_s^*(r_o, z_o) = \begin{cases} \dfrac{1}{\pi\left(r_H^2 - r_L^2\right)(z_H - z_L)} & r_L \le r_o \le r_H, \quad z_L \le z_o \le z_H \\ \\ 0 & \text{otherwise} \end{cases}$$

where r_L, r_H, z_L, z_H are constants as defined by the discretized forward problem. If the discretized error function is defined as $e(r,z)|_{r_L,z_L}^{r_H,z_H} = e(r_o, z_o) = \text{constant}$, then the response of interest is defined as

$$\langle Q_s^*(r_o, z_o) e(r,z) \rangle = \int_0^R 2\pi r dr \int_0^H dz \left(Q_s^*(r_o, z_o) e(r,z)\right)$$

$$= \frac{1}{\pi\left(r_H^2 - r_L^2\right)(z_H - z_L)} \left[\frac{2\pi r^2}{2} z e(r_o, z_o)\right]_{r_L,z_L}^{r_H,z_H} = e(r_o, z_o)$$

which is consistent with evaluating the error metric at location r_o, z_o.

An analytic solution to the adjoint equations with a step function source condition $Q_s^*(r_o, z_o)$ can be found by using the previously determined Green's function and evaluating the following convolution

$$\bar{T}^*(r,z) = \int_0^R 2\pi r_o dr_o \int_0^H dz_o \left(Q_s^*(r_o, z_o) \bar{T}^*(r_o, z_o \to r, z)\right)$$

Rewriting $\bar{T}^*(r_o, z_o \to r, z) = \begin{bmatrix} T_f^*(r_o, z_o \to r, z) & T_c^*(z_o \to z) \end{bmatrix}^T$ and $Q_s^*(r_o, z_o)$ using heaviside step functions results in the following expressions

$$T_f^*(r_o, z_o \to r, z) = \left[1 - H\left(z - z_o\right)\right] c_1 + \left[c_o + H\left(r - r_o\right) \tilde{c}_1 \ln\left(\frac{r}{r_o}\right)\right] \delta\left(z - z_o\right)$$

$$T_c^*(z_o \to z) = \left[1 - H(z - z_o)\right] c_1$$

$$Q_s^*(r_o, z_o) = H(r_o - r_L)[1 - H(r_o - r_H)] H(z_o - z_L)[1 - H(z_o - z_H)] \left[\frac{1}{\pi\left(r_H^2 - r_L^2\right)(z_H - z_L)}\right]$$

Examining each piece of the convolution:

$$\int_0^R 2\pi r_o dr_o \int_0^H dz_o Q_s^*(r_o, z_o) \left[1 - H\left(z - z_o\right)\right] c_1$$

$$= \begin{cases} 0, & z > z_H \\ \int_{r_L}^{r_H} 2\pi r_o dr_o \int_z^{z_H} dz_o \dfrac{c_1}{\pi\left(r_H^2 - r_L^2\right)\left(z_H - z_L\right)}, & z_H \geq z > z_L \\ \int_{r_L}^{r_H} 2\pi r_o dr_o \int_{z_L}^{z_H} dz_o \dfrac{c_1}{\pi\left(r_H^2 - r_L^2\right)\left(z_H - z_L\right)}, & z \leq z_L \end{cases}$$

$$= \begin{cases} 0, & z > z_H \\ \dfrac{\pi\left(r_H^2 - r_L^2\right)\left(z_H - z\right)}{\pi\left(r_H^2 - r_L^2\right)\left(z_H - z_L\right)} c_1 & z_H \geq z > z_L \\ \dfrac{\pi\left(r_H^2 - r_L^2\right)\left(z_H - z_L\right)}{\pi\left(r_H^2 - r_L^2\right)\left(z_H - z_L\right)} c_1 & z \leq z_L \end{cases}$$

$$= \begin{cases} 0, & z > z_H \\ \dfrac{\left(z_H - z\right)}{\left(z_H - z_L\right)} c_1 & z_H \geq z > z_L \\ c_1 & z \leq z_L \end{cases}$$

$$\int_0^R 2\pi r_o dr_o \int_0^H dz_o Q_s^*(r_o, z_o) c_o \delta(z - z_o)$$

$$= \int_{r_L}^{r_H} 2\pi r_o dr_o \int_0^H dz_o \frac{H(z_o - z_L)[1 - H(z_o - z_H)]}{\pi\left(r_H^2 - r_L^2\right)\left(z_H - z_L\right)} c_o \delta(z - z_o)$$

$$= \int_{r_L}^{r_H} 2r_o dr_o \frac{1}{(z_H - z_L)(r_H^2 - r_L^2)} H(z - z_L)\left[1 - H(z - z_H)\right]\left[\tilde{c}_1 \ln r_o + \frac{1}{2\pi}\left(\frac{1}{hR} + \frac{1}{k_f}\ln R\right)\right]$$

$$= \frac{1}{2\pi hR(z_H - z_L)} + \frac{\tilde{c}_1}{(z_H - z_L)(r_H^2 - r_L^2)}\left[r_H^2 \ln\left(\frac{r_H}{R}\right) - \frac{r_H^2}{2} - r_L^2 \ln\left(\frac{r_L}{R}\right) + \frac{r_L^2}{2}\right], \quad z_L \le z \le z_H$$

$$\int_0^R 2\pi r_o dr_o \int_0^H dz_o Q_s^*(r_o, z_o) H\left(r - r_o\right)\tilde{c}_1 \ln\left(\frac{r}{r_o}\right)\delta\left(z - z_o\right)$$

$$= \begin{cases} \int_{r_L}^{r} 2\pi r_o dr_o \int_0^H dz_o \dfrac{H(z_o - z_L)[1 - H(z_o - z_H)]}{\pi\left(r_H^2 - r_L^2\right)(z_H - z_L)}\tilde{c}_1 \ln\left(\dfrac{r}{r_o}\right)\delta\left(z - z_o\right), & r_L \le r < r_H \\ \int_{r_L}^{r_H} 2\pi r_o dr_o \int_0^H dz_o \dfrac{H(z_o - z_L)[1 - H(z_o - z_H)]}{\pi\left(r_H^2 - r_L^2\right)(z_H - z_L)}\tilde{c}_1 \ln\left(\dfrac{r}{r_o}\right)\delta\left(z - z_o\right), & r \ge r_H \end{cases}$$

$$= \begin{cases} \dfrac{H(z - z_L)[1 - H(z - z_H)]}{\left(r_H^2 - r_L^2\right)(z_H - z_L)}\tilde{c}_1\left(-r_L^2 \ln\left(\dfrac{r}{r_L}\right) + \dfrac{r^2 - r_L^2}{2}\right), & r_L \le r < r_H \\ \dfrac{H(z - z_L)[1 - H(z - z_H)]}{\left(r_H^2 - r_L^2\right)(z_H - z_L)}\tilde{c}_1\left(r_H^2 \ln\left(\dfrac{r}{r_H}\right) - r_L^2 \ln\left(\dfrac{r}{r_L}\right) + \dfrac{r_H^2 - r_L^2}{2}\right), & r \ge r_H \end{cases}$$

Therefore, the solution for $\bar{T}^*(r,z)$ using the above definition for $Q_s^*(r_o,z_o)$ is

$$T_f^*(r,z) = \begin{cases} 0 & 0 \le r \le R, \quad z_H < z \le H \\ c_1 & 0 \le r \le R, \quad 0 \le z < z_L \\ \left[\begin{array}{l} \dfrac{(z_H - z)}{(z_H - z_L)} c_1 + \dfrac{1}{2\pi h R (z_H - z_L)} + \\ \\ \dfrac{1}{2\pi k_f (z_H - z_L)\left(r_H^2 - r_L^2\right)} \left(\begin{array}{l} r_H^2 \ln\left(\dfrac{R}{r_H}\right) \\ -r_L^2 \ln\left(\dfrac{R}{r_L}\right) \\ +\dfrac{r_H^2 - r_L^2}{2} \end{array} \right) \end{array} \right] & 0 \le r < r_L, \quad z_L \le z \le z_H \\ \left[\begin{array}{l} \dfrac{(z_H - z)}{(z_H - z_L)} c_1 + \dfrac{1}{2\pi h R (z_H - z_L)} + \\ \\ \dfrac{1}{2\pi k_f (z_H - z_L)\left(r_H^2 - r_L^2\right)} \left(\begin{array}{l} r_H^2 \ln\left(\dfrac{R}{r_H}\right) \\ -r_L^2 \ln\left(\dfrac{R}{r}\right) \\ +\dfrac{r_H^2 - r^2}{2} \end{array} \right) \end{array} \right] & r_L \le r < r_H, \quad z_L \le z \le z_H \\ \dfrac{(z_H - z)}{(z_H - z_L)} c_1 + \\ \dfrac{1}{2\pi h R (z_H - z_L)} + \dfrac{1}{2\pi k_f (z_H - z_L)} \ln\left(\dfrac{R}{r}\right) & r_H \le r \le R, \quad z_L \le z \le z_H \end{cases}$$

$$T_c^*(z) = \begin{cases} 0 & z_H < z \leq H \\ c_1 & 0 \leq z < z_L \\ \dfrac{(z_H - z)}{(z_H - z_L)} c_1 & z_L \leq z \leq z_H \end{cases}$$

This solution is then integrated according to the inner product $\left\langle \bar{T}^*, \bar{r} \right\rangle_{r,z}$ using the same definition for the residual as before in the analytic error metric section with $\tilde{T} = b_o$. Examining the case where $0 \leq r \leq R,\ 0 \leq z < z_L$

$$\int_0^R 2\pi r dr \int_0^{z_L} dz \left[-q''' c_1 \right] = -q''' \pi R^2 z_L c_1$$

Examining the inner product with $0 \leq r < r_L,\ z_L \leq z \leq z_H$

$$\int_0^{r_L} 2\pi r dr \int_{z_L}^{z_H} dz \left[-q''' \left(\frac{(z_H - z)}{(z_H - z_L)} c_1 + \frac{1}{2\pi h R (z_H - z_L)} \right) \right]$$

$$+ \int_0^{r_L} 2\pi r dr \int_{z_L}^{z_H} dz \left[-q''' \left(\frac{r_H^2 \ln\left(\frac{R}{r_H}\right) - r_L^2 \ln\left(\frac{R}{r_L}\right) + \frac{r_H^2 - r_L^2}{2}}{2\pi k_f \left(z_H - z_L\right)\left(r_H^2 - r_L^2\right)} \right) \right]$$

$$= -q''' \left[r_l^2 \pi z_H c_1 - r_L^2 \pi c_1 \frac{z_H + z_L}{2} + \frac{r_L^2}{2hR} \right]$$

$$-q''' r_L^2 \left(\frac{r_H^2 \ln\left(\frac{R}{r_H}\right) - r_L^2 \ln\left(\frac{R}{r_L}\right) + \frac{r_H^2 - r_L^2}{2}}{2k_f \left(r_H^2 - r_L^2\right)} \right)$$

Examining the inner product with $r_L \leq r \leq r_H,\ z_L \leq z \leq z_H$

$$-q''' \left[(r_H^2 - r_L^2)\pi z_H c_1 - (r_H^2 - r_L^2)\pi c_1 \frac{z_H^2 - z_L^2}{2\left(z_H - z_L\right)} + \frac{(r_H^2 - r_L^2)}{2hR} \right]$$

$$+\int_{r_L}^{r_H} 2\pi r dr \int_{z_L}^{z_H} dz \left[-q''' \left(\frac{r_H^2 \ln\left(\frac{R}{r_H}\right) - r_L^2 \ln\left(\frac{R}{r}\right) + \frac{r_H^2 - r^2}{2}}{2\pi k_f \left(z_H - z_L\right)\left(r_H^2 - r_L^2\right)} \right) \right]$$

$$= -q''' \left[(r_H^2 - r_L^2)\pi z_H c_1 - (r_H^2 - r_L^2)\pi c_1 \frac{z_H + z_L}{2} + \frac{(r_H^2 - r_L^2)}{2hR} \right]$$

$$-q''' \left[\frac{r_H^2 \ln\left(\frac{R}{r_H}\right) + \frac{r_H^2}{2}}{2k_f} \right] + \frac{q'''}{8k_f}\left(r_H^2 + r_L^2\right)$$

$$-\frac{q''' r_L^2}{4k_f(r_H^2 - r_L^2)} \left[2r_H^2 \ln\left(\frac{r_H}{R}\right) - 2r_L^2 \ln\left(\frac{r_L}{R}\right) - (r_H^2 - r_L^2) \right]$$

Examining the inner product with $r_H < r \leq R,\ z_L \leq z \leq z_H$

$$-q''' \left[(R^2 - r_H^2)\pi z_H c_1 - (R^2 - r_H^2)\pi c_1 \frac{z_H + z_L}{2} + \frac{(R^2 - r_H^2)}{2hR} \right]$$

$$-q''' \int_{r_H}^{R} 2\pi r dr \int_{z_L}^{z_H} dz \frac{1}{2\pi k_f \left(z_H - z_L\right)} \ln\left(\frac{R}{r}\right)$$

$$= -q''' \left[(R^2 - r_H^2)\pi z_H c_1 - (R^2 - r_H^2)\pi c_1 \frac{z_H + z_L}{2} + \frac{(R^2 - r_H^2)}{2hR} \right]$$

$$-\frac{q'''}{4k_f} \left[2r_H^2 \ln\left(\frac{r_H}{R}\right) + (R^2 - r_H^2) \right]$$

Summing these parts together, we have for $\left\langle \bar{T}^*, \bar{r} \right\rangle_{r,z}$ the expression

$$\left\langle \bar{T}^*, \bar{r} \right\rangle_{r,z} = -q'''\pi R^2 c_1 \frac{(z_H - z_L)}{2} - q''' \frac{R}{2h} + \frac{q'''}{8k_f}\left(r_H^2 + r_L^2 - 2R^2\right)$$

This solution for the analytic adjoint using a step function source was compared with the mathematical and physical adjoint solutions. The comparison can be found in Numerical Results, Chapter 3 of this thesis.

2.2.4 Low Fidelity Adjoint Problem

Initially, the Adaptive Model Refinement project intended to use low fidelity adjoint solution based upon coarsened meshes and adjusted thermal conductivity values as a means of predicting the difference between high and low fidelity models. During numerical testing, this method was shown to lack adequate predictive capability of the quantities of interest. In general, adjoint solutions contain information regarding the local temporal and spatial importance of the residual regarding a specific quantity of interest. The devolution of the mesh from high to low skewed this local importance such that the estimated quantity of interest no longer held pertinent information in regards to the accuracy of the low fidelity model.

Solving for the low fidelity mathematical adjoint is the same as solving for the high fidelity mathematical adjoint using $\widetilde{\bar{\mathbf{A}}}^* = \widetilde{\bar{\mathbf{A}}}^T$ in place of $\bar{\mathbf{A}}^*$. However, in order to evaluate the response $\widetilde{\Re} = \left\langle \widetilde{T}^\dagger, \bar{r} \right\rangle$, the adjoint solution $\widetilde{T}^\dagger$ must be projected onto the high fidelity mesh in order to determine the inner product. This elongation process is non-unique, and a variety of methods were considered to arrive at a low fidelity adjoint solution extrapolated to the high fidelity mesh.

One method considers an additional linear set of equations for the low-fidelity problem. Rewriting the low fidelity equation (2.7)

$$\widetilde{\bar{\mathbf{C}}}_{n+1}\widetilde{\boldsymbol{\phi}}_{n+1} = \widetilde{\bar{\mathbf{B}}}_{n+1}\widetilde{\boldsymbol{\phi}}_n - \widetilde{\mathbf{Q}}_{n+1},$$

we have an additional set of linear equations that project the low fidelity temperatures onto the high fidelity mesh

$$\widetilde{\bar{\mathbf{E}}}\widetilde{\boldsymbol{\phi}}_{n+1} = \bar{\bar{\mathbf{I}}}\widetilde{\boldsymbol{\theta}}_{n+1} \tag{2.13}$$

where $\widetilde{\boldsymbol{\theta}}_{n+1}$ is the low fidelity temperature projected onto the high fidelity mesh and the $\widetilde{\bar{\mathbf{E}}}_{n+1}$ is a $m \times n$ operator with $n > m$ that linearly interpolates the $\widetilde{\boldsymbol{\phi}}_{n+1}$ vector. Writing the block matrix time structure of this problem

$$\begin{bmatrix}
\widetilde{\bar{\mathbf{C}}}_1 & & & & & & & \\
\widetilde{\bar{\mathbf{E}}} & -\bar{\bar{\mathbf{I}}} & & & & & & \\
\widetilde{\bar{\mathbf{B}}}_2 & & \widetilde{\bar{\mathbf{C}}}_2 & & & & & \\
 & & \widetilde{\bar{\mathbf{E}}} & -\bar{\bar{\mathbf{I}}} & & & & \\
 & & & \ddots & & & & \\
 & & & & \widetilde{\bar{\mathbf{B}}}_N & \widetilde{\bar{\mathbf{C}}}_N & & \\
 & & & & & \widetilde{\bar{\mathbf{E}}} & -\bar{\bar{\mathbf{I}}}
\end{bmatrix}
\begin{bmatrix}
\widetilde{\boldsymbol{\phi}}_1 \\ \widetilde{\boldsymbol{\theta}}_1 \\ \widetilde{\boldsymbol{\phi}}_2 \\ \widetilde{\boldsymbol{\theta}}_2 \\ \vdots \\ \widetilde{\boldsymbol{\phi}}_N \\ \widetilde{\boldsymbol{\theta}}_N
\end{bmatrix} =
\begin{bmatrix}
\widetilde{\mathbf{Q}}_1 \\ 0 \\ \widetilde{\mathbf{Q}}_2 \\ 0 \\ \vdots \\ \widetilde{\mathbf{Q}}_N \\ 0
\end{bmatrix}$$

Transposing the matrix operator for the time dependent adjoint equation set and selecting $\widetilde{Q}^*$ as now noted produces

$$\begin{bmatrix} \widetilde{\bar{\mathbf{C}}}_1^* & \widetilde{\bar{\mathbf{E}}}^* & \widetilde{\bar{\mathbf{B}}}_2^* & & & & & \\ & -\bar{\bar{\mathbf{I}}} & & & & & & \\ & & \widetilde{\bar{\mathbf{C}}}_2^* & \widetilde{\bar{\mathbf{E}}}^* & \widetilde{\bar{\mathbf{B}}}_3^* & & & \\ & & & -\bar{\bar{\mathbf{I}}} & & & & \\ & & & \ddots & & & & \\ & & & & & \widetilde{\bar{\mathbf{C}}}_N^* & \widetilde{\bar{\mathbf{E}}}^* & \\ & & & & & & -\bar{\bar{\mathbf{I}}} & \end{bmatrix} \begin{bmatrix} \widetilde{\boldsymbol{\phi}}_1^* \\ \widetilde{\boldsymbol{\theta}}_1^* \\ \widetilde{\boldsymbol{\phi}}_2^* \\ \widetilde{\boldsymbol{\theta}}_2^* \\ \vdots \\ \widetilde{\boldsymbol{\phi}}_N^* \\ \widetilde{\boldsymbol{\theta}}_N^* \end{bmatrix} = \begin{bmatrix} 0 \\ \widetilde{\mathbf{Q}}_1^* \\ 0 \\ \widetilde{\mathbf{Q}}_2^* \\ \vdots \\ 0 \\ \widetilde{\mathbf{Q}}_N^* \end{bmatrix}$$

Note for a single time step, we have the following adjoint matrix equations

$$\widetilde{\bar{\mathbf{C}}}_n^* \widetilde{\boldsymbol{\phi}}_n^* + \widetilde{\bar{\mathbf{E}}}^* \widetilde{\boldsymbol{\theta}}_n^* + \widetilde{\bar{\mathbf{B}}}_{n+1}^* \widetilde{\boldsymbol{\phi}}_{n+1}^* = 0$$

$$-\bar{\bar{\mathbf{I}}} \widetilde{\boldsymbol{\theta}}_n^* = \widetilde{\mathbf{Q}}_n^*$$

where $\bar{\mathbf{Q}}^*$ is the same right hand side as for the mathematical adjoint. The previous system of linear equations reveals that $\widetilde{\boldsymbol{\theta}}_{n+1}^* = -\widetilde{\mathbf{Q}}$ which implies that $\widetilde{\mathbf{Q}}^*$ should be selected equal to $\bar{\mathbf{Q}}^*$. The system then simply solves the low fidelity adjoint problem with $\bar{\mathbf{Q}}^*$ volume weighted to the low fidelity mesh. The resulting expression for $\widetilde{\boldsymbol{\theta}}_{n+1}^*$ will contain no information with regards to the adjoint solution $\widetilde{\boldsymbol{\phi}}_{n+1}^*$, and the resulting response integral is trivial.

Another attempt at arriving at an effective low fidelity adjoint solution used the same operator $\widetilde{\bar{\mathbf{E}}}_{n+1}$ to linearly interpolate the low fidelity adjoint solution onto the high fidelity mesh in a similar fashion to the forward low fidelity problem. This, however, also resulted in response functions that did not accurately describe the differences between the high and low fidelity fuel temperatures.

Chapter 3

Numerical Results

This chapter examines the numerical behavior of the forward and adjoint problems. Various figures and descriptions are given analyzing the forward low and high fidelity solution behaviors as well as adjoint solution behavior. The effectiveness of the physical, mathematical, and analytic adjoint solutions' prediction of the quantity of interest is also investigated in the following chapter.

3.1 Numerical Results for Forward Problem

Figure 3.1 below contains the temperature profile for the steady state solution of the forward problem, equations (2.8) and (2.9), using the high fidelity finite differencing scheme, the low fidelity lumped parameter and finite differencing scheme, and the linear interpolation used to project the low fidelity solution onto the high fidelity geometry. The solutions are shown for a given axial location that is halfway up the height of the fuel pin with a high fidelity ring number of 8 and a low fidelity ring number of 4. Heat generation is assumed constant across the radial direction of the pin at this given axial location.

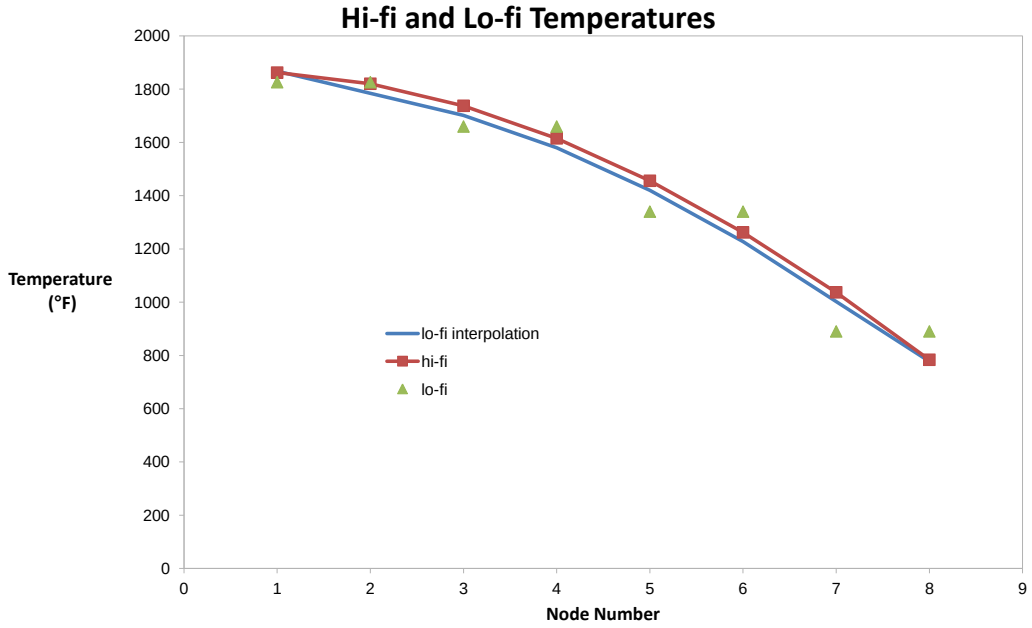

Figure 3.1: **Steady state forward solution as determined by the low fidelity, high fidelity, and low-to-high linear interpolation solution methods**

The red series that represents the high fidelity solution exhibits the quadratic structure that we would expect for a constant heat generation problem. The green series in Figure 3.1 shows the coarsened finite difference model with half as many radial nodes as the high fidelity problem. The adjusted parameters calculated with equation (2.4), when used with the low fidelity problem, will result in exactly the same volume averaged temperatures as the high fidelity problem. The linear interpolation of the low fidelity onto the high fidelity geometry will however contain differences in temperature. The blue line in Figure 3.1 shows the linear interpolation of the low fidelity solution onto the high fidelity mesh. These temperature differences or ΔTs are the quantity of interest for both the steady state and time dependent examples. The differences are noted to be small (2.1% of the largest relative error shown in Figure 3.1). Four linear regions can be seen between the green low fidelity regions, and a small difference between the blue line and the red series can be seen for almost every high fidelity temperature node.

The time dependent forward problem exhibits low fidelity and high fidelity volume averaged temperatures that are not exact. This is due to the fact that the lumped parameters as deter-

mined by equations (2.4) and (2.5) use the steady state forward temperature rather than the time dependent values. Figure 3.2 shows the time dependent behavior at a given axial and radial location within the pin for the low fidelity solution verses the high fidelity solution coarsened to the low fidelity mesh.

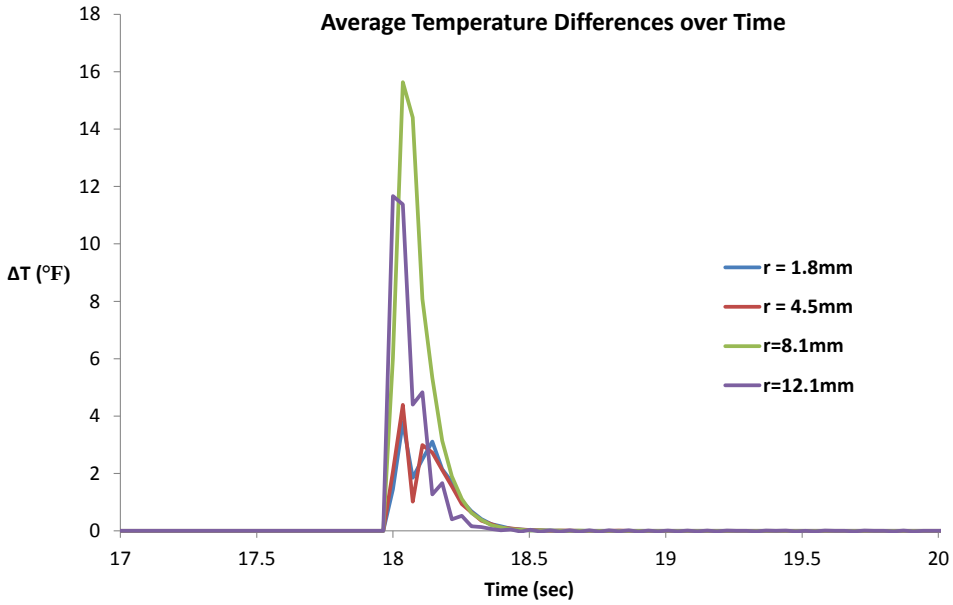

Figure 3.2: **Difference in time dependent hi-fi and low fidelity solution average temperatures at four separate locations of interest**

The results presented in Figure 3.2 correspond to a high fidelity ring number of 8, a low fidelity ring number of 4, and an axial mesh number of 20. The figure shows the ΔT difference between the volume averaged high fidelity solution and the low fidelity solution at each time step. At $t = 0.005$ hrs, the heat generation within the pin is reduced by a factor of 4. Prior to this heat generation step, the k_{eff} and h_{eff} values as determined by equations (2.4) and (2.5) to ensure that the volume averaged high fidelity solution and the low fidelity solution are equal. Once the q''' jump has occurred, the k_{eff} and h_{eff} values for the pseudo-steady state forward problem no longer ensure that $\Delta T = 0$ as one can see from the figure. After the transient has subsided, the difference between the high fidelity volume averaged solution and low fidelity solution return to zero. Each line in Figure 3.2 represents a different low fidelity radial location.

All radial locations correspond to an axial location halfway up the pin.

3.2 Numerical Adjoint Behavior

Using the high fidelity mathematical adjoint for either the time dependent or steady state problem yields the exact value for the quantity of interest at every axial and radial location regardless of the mesh size. The time dependent shape of the mathematical adjoint solution is rather unique given its role as an indicator of the relative influence exerted on the temperature difference at a particular location of interest. Figures 3.3 through 3.5 show the time dependent nature of the high fidelity adjoint.

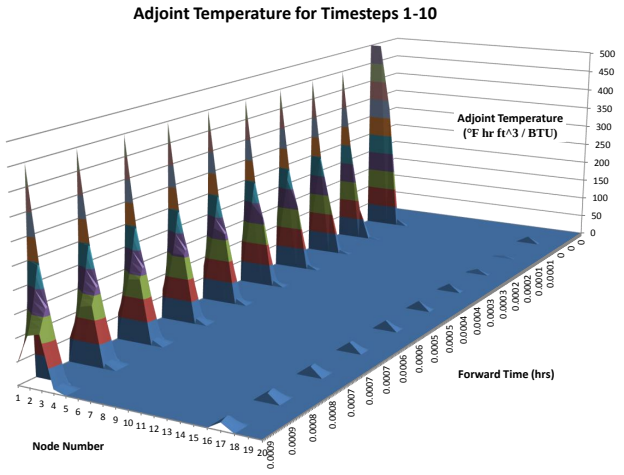

Figure 3.3: **Hi-fi adjoint time dependent solution shape for timesteps 1-10**

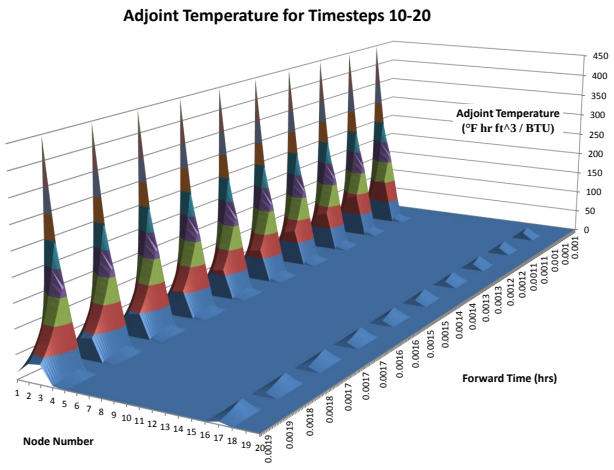

Figure 3.4: **Hi-fi adjoint time dependent solution shape for timesteps 10-20**

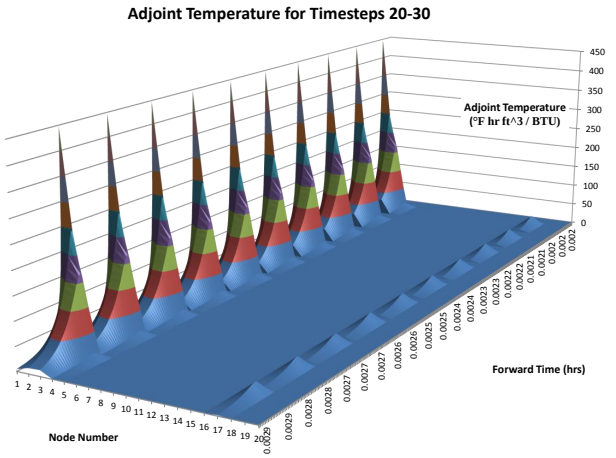

Figure 3.5: **Hi-fi adjoint time dependent solution shape for timesteps 20-30**

Figures 3.3 through 3.5 are for a location of interest at the first radial and first axial node with a ring number of 8 and a radial mesh of 8. The time steps were 0.0001 hours or 0.36 seconds. "Forward time" refers to a fixed Q^* location in time. Both adjoint time and forward time are increasing along the time axis in Figures 3.3 - 3.5 with forward time values listed along the axis. Each adjoint time node contains 30 forward time nodes, since a full temporal and spatial distribution of adjoint values is necessary to calculate the inner product for a given forward

time value. This adjoint time behavior can be seen by observing the T^* shape along the time axis during which the forward time remains constant. Each mathematical adjoint solution will have a given "adjoint time" dependent shape for a constant value of "forward time."

The node number denotes all spatial nodes for every axial and radial location including the axial coolant nodes. Node ordering has the radial values for the first axial location followed by the radial values for the second axial location and so on. Since the first axial mesh is the location of interest, its values are nonzero in the previous figures while the other axial locations are zero with the exception of the coolant values. One can conclude from this that, since there is no axial coupling conduction model for the fuel, other axial mesh locations exhibit no influence on the ΔT quantity of interest. It's also important to note that while the coolant does have some influence, its adjoint solution value is considerably lower than the fuel ring adjoint values.

With the exception of $t = 0.00$, all times steps have the same relative shape with regards to adjoint time. As forward time increases, the location of interest in adjoint time shifts so that more and more of the time dependent adjoint solution shape is revealed. It can be seen that the adjoint solution spikes at the location of interest and then begins to decay away. One can conclude that for a given ΔT, the temperatures at the same time as the examined quantity of interest exhibit the greatest influence on the evaluated metric. Earlier times also exhibit some influence on the quantity of interest, but this influence decays away the farther one is from the time of interest. These figures also demonstrate that future time temperature values have zero influence on a given ΔT.

A time integrated adjoint solution was investigated for several times of interest to better understand the differences between the high fidelity and low fidelity solution shapes. The time integrated adjoints were determined according to the following equation

$$\begin{aligned} T_{hi} - T_{lo} = \Delta T(t_f) &= \int_0^{t_f} dt \int_V d^3r \cdot R(\vec{r}) \cdot T^*(\vec{r}, t) \\ &= \int_V d^3r \cdot R(r, z) \int_0^{t_f} dt \cdot T^*(r, z, t) \\ &= \int_V d^3r \cdot R(r, z) \left\langle T^*(r, z) \right\rangle_{t_f} \end{aligned} \tag{3.1}$$

Because the residuals $R(r, z)$ are assumed to be time independent, equation (3.1) only holds for pseudo-steady state conditions such that q''' is unchanged. Figure 3.6 shows time integrated

$\langle T^*(r,z)\rangle_{t_f}$ values as defined by equation (3.1) for high and low fidelities at three separate t_f times of interest.

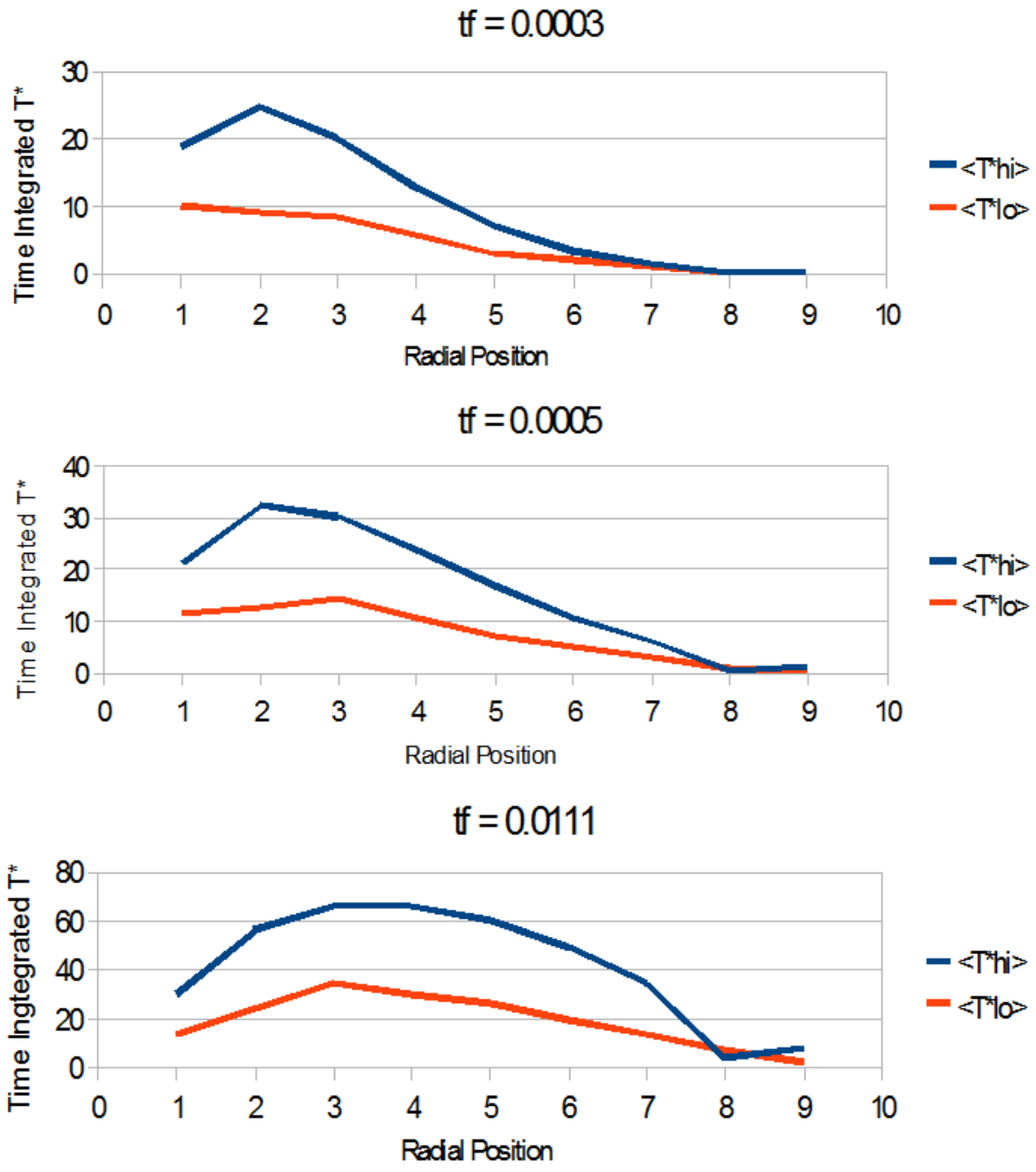

Figure 3.6: **Time integrated T^* for low and high fidelities for given t_f values**

In each case, the location of interest was the centerline radial value and the first axial location or bottom of the fuel pin. The high fidelity ring number was 8 and the low fidelity ring number was 4. There are some similarities between the two adjoint solution shapes, but the low fidelity adjoint is consistently less than the high fidelity adjoint. Since the residuals used in both error metrics are the same, the low fidelity adjoint solution will therefore predict a drastically different response than the high fidelity adjoint solution.

3.3 Numerical Determination of the Quantity of Interest

The following section outlines the various results for the evaluation of a given quantity interest using adjoints. Quantities of interest typically are differences between low-fidelity and high fidelity solutions at a particular location within the fuel pin. It was found that for time dependent problems, the mathematical adjoint predicted perfectly the difference between low and high fidelity problems for either time dependent, steady state, or pseudo-steady state problems at every location of interest within the fuel pin. Initial investigation of the low fidelity adjoint's best estimate of the quantity of interest showed inaccurate approximations, and it was deemed unable to accurately predict the difference between high and low fidelity temperatures in the time dependent problem and steady state problems alike.

Since low fidelity approximations exhibited erratic behavior for the time dependent cases, the problem was simplified to pseudo-steady state cases using constant heat generation and steady state cases with no time dependency whatsoever. Even for these cases, the low fidelity adjoint response does not return accurate approximations of the quantity of interest. The response estimated by the adjoint solutions is the total sum of each adjoint value multiplied by each corresponding nodal residual for a given time step. This residual summation behavior was investigated to gain an understanding of what was occurring during the low fidelity adjoint approximation. Time index in the following figures pertains to both forward time and adjoint reverse time. Each index value corresponds to a fixed location in forward time and all subsequent values in reverse time. Therefore, each "peak" denotes a single location in forward time swept through all adjoint reverse time values. Index values are simply marking the time dependent behavior in both forward and adjoint time. The following figures demonstrate the pseudo-steady state behavior using high and low fidelity adjoint approximations.

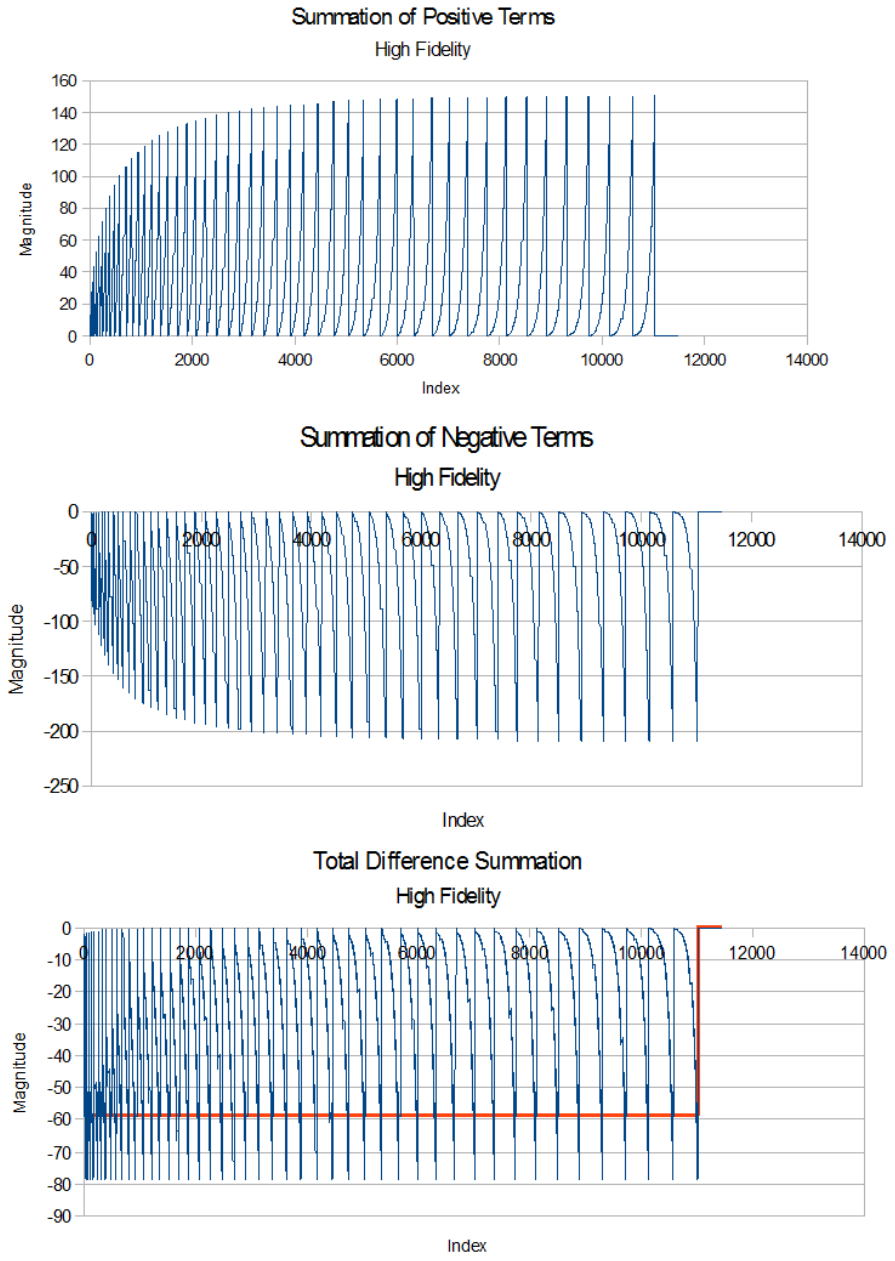

Figure 3.7: **Collection of discretized $\langle T^*_{hi}, r \rangle_{r,z,t}$ positive and negative values as well as their summation and its resulting estimate of the quantity of interest**

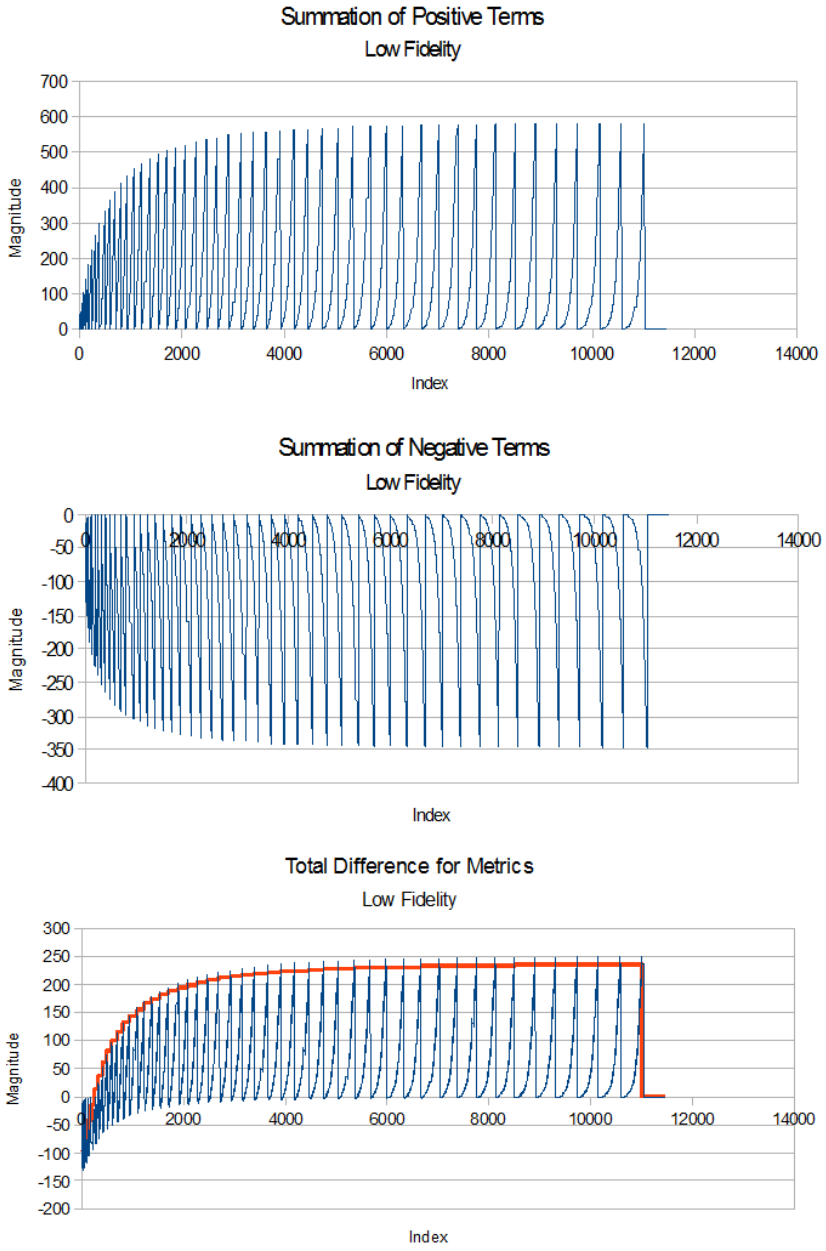

Figure 3.8: **Collection of discretized $\langle T^*_{lo}, r \rangle_{r,z,t}$ positive and negative values as well as their summation and its resulting estimate of the quantity of interest**

The location of interest corresponds to the centerline of the fuel pin and the first axial location. The low fidelity estimate of 248^oF in figure 3.8 is drastically different than the high fidelity's estimate of -59^oF in figure 3.7. The constant value predicted by the high fidelity adjoint is consistent with the constant difference found between the linearly interpolated low fidelity forward problem and the high fidelity forward problem for the pseudo-steady state case. In these figures, the x-axis index denotes the axial and radial node indices along with the time-step index, and the y-axis represents the inner product summation up to a specific index value. Each spike in these figures corresponds to the summation for a specific time of interest. It is interesting to note that although the positive and negative terms approach asymptotic maximum values in figure 3.7, the estimated quantity of interest remains constant. In figure 3.8 however, it takes several time steps for the estimated quantity of interest to reach a constant value. This phenomenon shows the sensitivity of the mathematical adjoint approximation of the quantity of interest and high fidelity mathematical adjoint's ability to predict the quantity of interest regardless of temporal behavior.

In order to verify the low fidelity adjoint, a"low-low" fidelity model was constructed. Comparing the low-fidelity to a "low-low" fidelity is effectively the same as comparing a high fidelity model to a low fidelity model. Therefore, the low fidelity adjoint should predict the exact difference between the low and "low-low" temperature calculations. The low-low fidelity problem considered was a constant temperature equal to the coolant inlet temperature. Figure 3.9 shows the ΔT values as evaluated by the low fidelity adjoint solution and low fidelity $< Q^*, e >$ inner product.

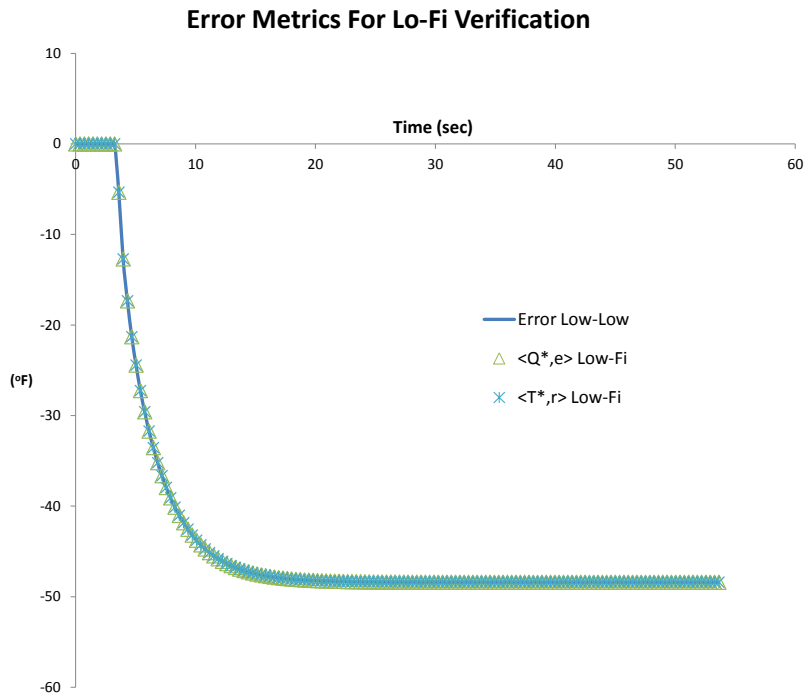

Figure 3.9: **Verification results for the low fidelity adjoint approximation using a steady state "low-low" fidelity solution**

Before the decrease in q''', the low and low-low fidelities are equal to each other and the resulting error metric is zero as seen in figure 3.9. At $t = 0.001$ hours, the low fidelity problem begins to deviate from the pseudo-steady state low-low problem since q''' is decreased at that time. The error metric approximated by the low-fidelity adjoint solution is consistent both with the $\langle Q^*, e \rangle$ inner product and the exact error between the low and low-low fidelity problems. This verifies that the low fidelity adjoint solution is correct and that the linear interpolation of the low fidelity adjoint solution onto the high fidelity spatial mesh is where the significant difference between low and high fidelity response occurs.

Initially, the physical and analytical adjoints showed erratic predictive behavior of the quantity of interest similar to that of the low fidelity adjoint. To contrast the quantity of interest calculated using the three adjoints, the forward problem was further simplified such that the low-fidelity was considered to be a constant temperature throughout the fuel and coolant and set to the coolant inlet temperature. Though completely incorrect, the forward boundary conditions were still satisfied. In this case, the physical and analytical adjoints were found to approximate

the quantity of interest exactly. Figure 3.10 below shows the adjoint solution shapes for three separate radial locations across the same axial location halfway up the fuel pin.

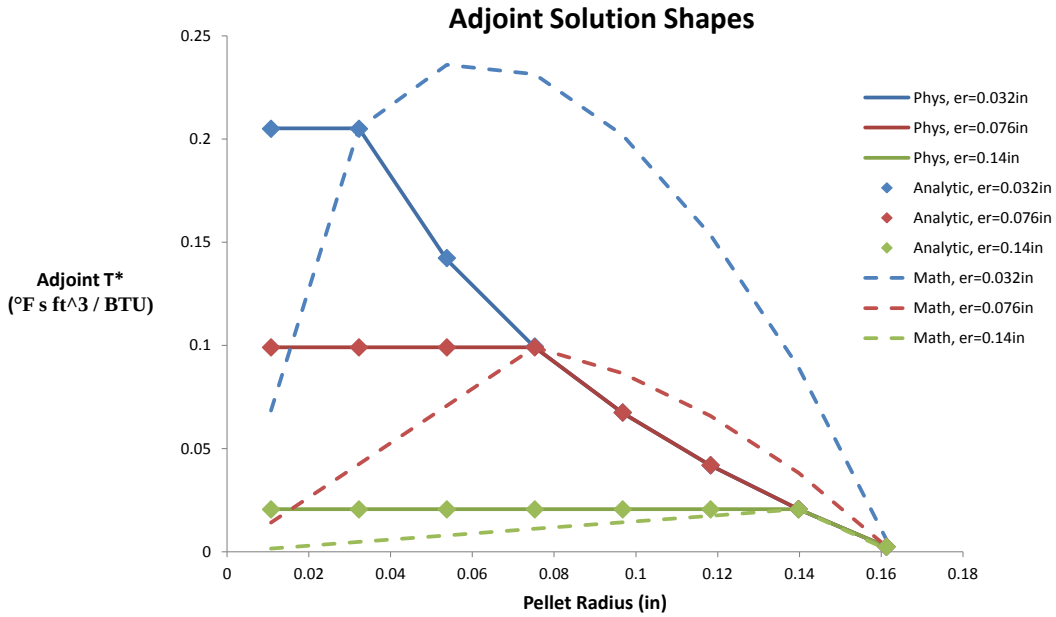

Figure 3.10: **Solution shapes for physical, analytical, and mathematical adjoints for three separate radial locations of interest**

The diamonds, corresponding to the analytical solution, match almost exactly the physical adjoint values. This solution shape has a constant value from the centerline up to the location of interest and decreases logarithmically thereafter. By contrast, the dotted line displays a dissimilar solution shape for the mathematical adjoint solution. At the location of interest it matches the physical and analytical value, but it shows linear and quadratic behavior before and after this radial point. For the case where the quantity of interest is at a radial location of 0.032 inches, the mathematical solution increases quadratically after the location of interest and then begins to diminish. For the other cases, the location of interest is where the maximum adjoint value occurs. Since T^* is a representation of the relative importance of a location with regards to the quantity of interest, figure 3.10 demonstrates that, according to the mathematical adjoint, regions at or after the location of interest are weighted more heavily than other locations. The physical and analytical adjoints, however, suggest that all temperature rings before the loca-

tion of interest are equally weighted and the importance of later rings decreases logarithmically.

Table 3.1 below shows the numerically evaluated quantities of interest corresponding to the same locations as shown previously in figure 3.10. Note that the quantity of interest being evaluated is the difference $T_{lo}(r,z) - T_{hi}$ where $T_{lo} = T_{c,inlet}$.

Table 3.1: **Physical, Analytical, and Mathematical Evaluations of the Quantity of Interest**

Inner Product	**er=0.032in**	**er=0.057in**	**er=0.14in**
$< T^*_{hi}, r >$	-1971.75 ^oF	-1577.39 ^oF	-591.50 ^oF
$< T^*_{phys}, r >$	-1971.75 ^oF	-1577.39 ^oF	-591.50 ^oF
$< T^*_{anylitic}, r >$	-1971.75 ^oF	-1577.39 ^oF	-591.50 ^oF
$< Q^*, e >$	-1971.75 ^oF	-1577.39 ^oF	-591.50 ^oF
$T_{lo} - T_{hi}$	-1971.75 ^oF	-1577.39 ^oF	-591.50 ^oF

As mentioned earlier, the analytical and physical adjoints produce the exact value for the quantity of interest when a constant low fidelity solution is used. The fact that non-constant values for the low fidelity solution result in incorrect analytical and physical adjoint approximations can be attributed to the fact that the residuals as determined by the forward operator are not consistent with those that would be determined using the transpose of the physical adjoint operator. In the case where the low fidelity forward solution is constant, all second order derivatives are equal to zero and the residuals defined by the transposed physical adjoint operator will be equal to the same residuals obtained by the mathematical forward operator.

The low fidelity adjoint mathematical solution shape was also compared to the high fidelity adjoint shape. Figure 3.11 shows the adjoint solution shape for the same locations of interest as in figure 3.10.

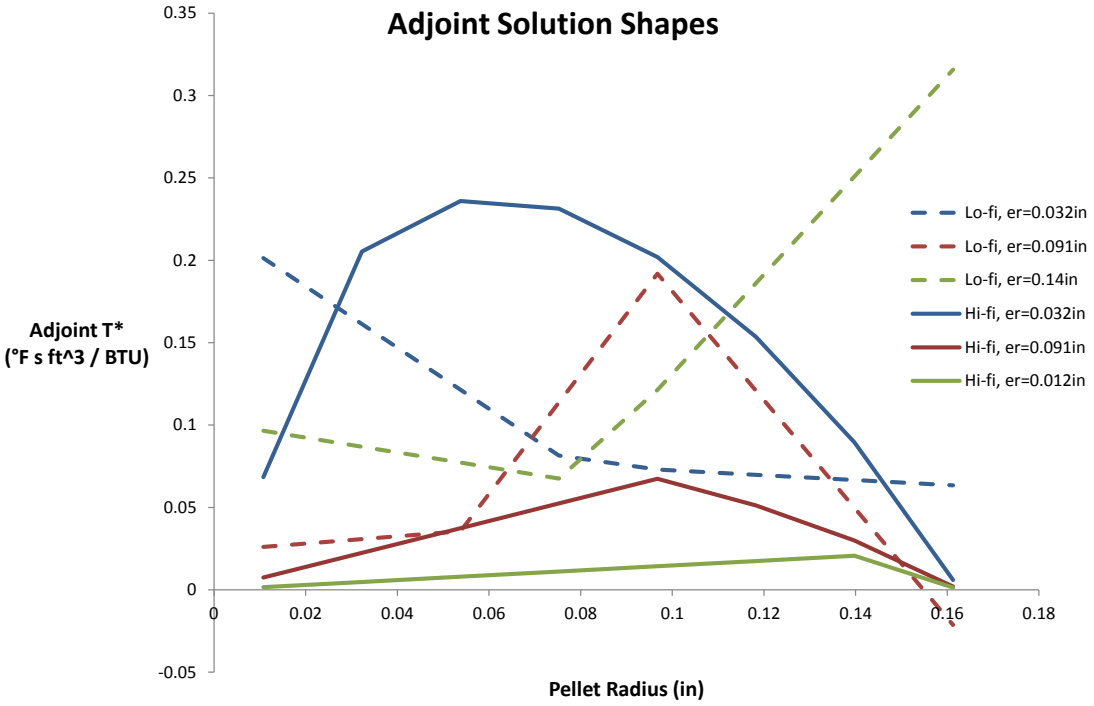

Figure 3.11: **Solution shapes for low fidelity and high fidelity mathematical adjoints for three separate radial locations of interest**

The high fidelity solution shapes in figure 3.11 are the same as previously shown in figure 3.10. The low fidelity solutions represented by the color coded dotted lines show highly erratic behavior with no indication of weighting the appropriate location of interest. Table 3.2 below shows the numerically evaluated quantities of interest corresponding to the same locations as shown previously in figure 3.11. In this case, the evaluated response is the difference between the high fidelity forward solution and the linearly interpolated low fidelity solution.

Table 3.2: **High and Low Fidelity Evaluations of the Quantity of Interest**

Inner Product	**er=0.032in**	**er=0.057in**	**er=0.14in**
$< T^*_{hi}, r >$	-65.73 ^oF	-65.73 ^oF	-41.08 ^oF
$< T^*_{lo}, r >$	213.54 ^oF	-592.54 ^oF	5380.72 ^oF
$< Q^*, e >$	-65.73 ^oF	-65.73 ^oF	-41.08 ^oF
$T_{lo} - T_{hi}$	-65.73 ^oF	-65.73 ^oF	-41.08 ^oF

Again, the mathematical solution approximates the difference exactly while the low fidelity solution exhibits highly erratic behavior inconsistent with an appropriate approximation.

Chapter 4

Conclusions and Future Work

4.1 Conclusion

In all cases, the mathematical adjoint was found to predict exactly the difference between the low fidelity and high fidelity temperatures regardless of whether the problem was time dependent or how the low fidelity temperatures were determined. Investigation of using the low fidelity mathematical adjoint in order to approximate the same QoI showed that low fidelity adjoint solutions were unable to predict quantities within acceptable tolerances. This conclusion was reinforced regardless of time dependence or low fidelity forward problem definition.

The physical and analytical adjoints were found to predict the proper quantities of interest for cases where the residuals obtained using physical and mathematical adjoint operators were consistent; namely, cases where the low fidelity coolant and fuel temperatures were constant. For this scenario, all spatial derivatives, including their discretized approximations, were zero. Although the physical and mathematical adjoint solution shapes varied drastically, the evaluated QoIs were still correct. The evaluation of the analytical adjoint solution provided a benchmark that verified the physical adjoint solution.

Given that the high fidelity adjoint appears to be necessary for the accurate evaluation of specific responses, there need to be adjusted conditions such that it would make sense to use an adjoint approach to support adaptive simulation. Note that the adjoint source term only depends on the QoI and not the forward source term, e.g. power density. This implies that whenever the QoI is to be evaluated, a high fidelity adjoint solution is required. If there are instances where one is interested in obtaining the forward solution for many different forward source terms, there may be a computational advantage of employing the adjoint approach to determine the QoI to judge whether the low fidelity forward solution being employed is suffi-

ciently accurate.

Although the low fidelity adjoint solution does not provide accurate estimations of temperature differences, a conclusion can be drawn with regards to adaptive model refinement. Because the mathematical adjoint gives the exact difference between a given fidelity and all lower fidelities, it can be used to estimate when a given fidelity converges to a higher level of fidelity. In other words, as the difference between a middle fidelity and lower model fidelity decreases, it is conjectured that the difference between the middle fidelity and high fidelity also decreases. This adaptive method can determine when to step up fidelity levels without actually solving for the high fidelity problem and is similar to methods used in adaptive grid refinement.

4.2 Future Work

The complexity of this problem could be increased for further study of the aforementioned low/mid/high fidelity difference estimations. Currently, for basic heat conduction and HEM heat convection, the differences between middle and high fidelities are small. Adding a more complex convection fluids model that includes radial and axial coolant nodes within a given channel could help demonstrate the adaptive model technique investigated in this thesis with more tangible results. Also adding axial coupling with regards to heat conduction could be another model fidelity level worth investigating using adaptive techniques along with varying fuel thermal conductivities with respect to temperature. Future work could also include an expression for the adjoint source, or response function, that results at the high fidelity level from the formulation of low fidelity adjoint equations. It may be possible to computationally derive this response function and could be interesting to contrast it with the true and desired high fidelity response function.

REFERENCES

[1] Jackson, C. J., D. G. Cacuci, and H. B. Finnemann. "Dimensionally Adaptive Neutron Kinetics for Multdimensional Reactor Safety Transients-I: New Features of RELAP5/PANBOX." *Nuclear Science and Engineering* Vol. 131 No. 2, 143-163 (1999).

[2] Jackson, C. J., D. G. Cacuci, and H. B. Finnemann. "Dimensionally Adaptive Neutron Kinetics for Multdimensional Reactor Safety Transients-II: Dimensionally Adaptive Switching Algorithms." *Nuclear Science and Engineering* Vol. 131 No. 2, 164-186 (1999).

[3] Williams, Mark L. "Perturbation Theory for Nuclear Reactor Analysis." *CRC Handbook of Nuclear Reactors Calculations* Vol. 3, 63-188 (1987).

[4] Pironneau, O. "On Optimum Design in Fluid Mechanics." *Journal of Fluid Mechanics* Vol. 64 part 1, 97-110 (1974).

[5] Pupko, V. Y. "Use of Adjoint Functions in Investigations of Heat Conduction and Transfer Processes." *Inzhenerno-Fizicheskii Zhurnal* Vol. 11 No. 2, 242-249 (1966).

[6] Dam, H. van, and J. E. Hoogenboom. "The Adjoint Space in Heat Transport Theory." *International Journal of Heat and Mas Transfer* Vol. 23, 349-353 (1980).

[7] Huang, C. H., and M. N. Ozisik. "Inverse Problem of Determining Unknown Wall Heat Flux in Laminar Flow Through a Parallel Plate Duct." *Numerical Heat Transfer* Part A Vol. 21, 55-70 (1992).

[8] Huang, C., S. Wang. "A Three-Dimensional Inverse Heat Conduction Problem in Estimating Surface Heat Flux by Conjugate Gradient Method." *International Journal of Heat and Mass Transfer*, Vol. 42, 3387-3403 (1999).

[9] *An Optimal Control Approach to A Posteriori Error Estimation in Finite Element Methods.* Institut fur Angewandte Mathematik, Universitat Heidelburg, (2001).

[10] Petersdorff, T. Von, and R. Leis. "Boundary Integral Equations for Mixed Dirichlet, Neumann and Transmission Problems." *Mathematical Methods in the Applied Sciences* Vol. 11, 185-213 (1989).

[11] Carey, V., D. Estep, A. Johansson, M. Larson, and S. Tavener. "Blockwise Adaptivity for Time Dependent Problems Based on Coarse Scale Adjoint Solutions." *SIAM Journal on Scientific Computing* Vol. 342 No. 4, (2010).

[12] Estep, D., S. Tavener, and T. Wildey. "A Posteriori Analysis and Improved Accuracy for an Operator Decomposition Solution of a Conjugate Heat Transfer Problem." *SIAM Journal on Numerical Analysis* Vol. 46 No. 4, 2068-2089 (2008).

[13] Estep, D., V. Ginting, D. Ropp, J. N. Shadid, and S. Tavener. "An A Posteriori - A Priori Analysis of Multiscale Operator Splitting." *Siam Journal on Numerical Analysis* Vol 46 No. 3, 1116-1146 (2008).

[14] Estep, D. M. Pernice, D. Pham, S. Tavener, and H. Wang. "A Posteriori Error Analysis of a Cell-Centered Finite Volume Method for Semilinear Elliptic Problems." *Journal of Computational and Applied Mathematics* Vol. 233, 459-472 (2009).

[15] Estep, D. M. Pernice, D. Pham, S. Tavener, and H. Wang. "A Posteriori Error Analysis for a Cut Cell Finite Volume Method." *Computational Methods in Applied Mechanics and Engineering* Vol. 200, 2768-2781 (2011).

[16] Yen, D. H. Y., J. V. Beck. "Green's Functions for Non-Self-Adjoint Problems in Heat Conduction with Steady Motion." *Journal of Engineering Mathematics* Vol. 57, 115-132 (2007).

[17] Versteeg, H. K., and W. Malalasekera. *An Introduction to Computational Fluid Dynamics: The Finite Volume Method*. Harlow, England: Pearson-Prentice Hall, 2007.

[18] Jarny, Y., M. N. Ozisik, and J. P. Bardon. "A General Optimization Method Using Adjoint Equation for Solving Multidimensional Inverse Heat Conduction." *International Journal of Heat and Mass Transfer* Vol. 34 No. 11, 2911-2919 (1991).

[19] Mesina, G. L.,"Reformulation RELAP5-3D in FORTRAN 95 and Results." *Proceedings of the ASME 2010 Joint US-European Fluids Engineering Summer Meeting and 8th International Conference on Nanochannels Microchannels, and Minichannels* , FEDSM2010-ICNMM2010, Montreal, Quebec, Canada, Aug 1-5, (2010).

[20] Martin, R. P. "TRAC-B thermal-Hydraulic Analysis of the Black Fox Boiling Water Reactor." *National Technical Information Service, 77H-Reactor Engineering and Nuclear Power Plants*. Issue 9318, 1993.

[21] Areva NP Inc, *COBRA-FLX: A Core Thermal-Hydraulics Analysis Code.* ANP-10311NP. pbadupws.nrc.gov, (2010).

[22] Sung, Y., R. L. Oelrich Jr., C. C. Lee, N. Ruiz-Esquide, M. Gambetta, and C. M. Mazufri, "Bechmark of Subchannel Code VIPRE-W with PSBT Void and Temperature Test Data." *Science and Technology of Nuclear Instalations*, Vol. 2012, (2012).

[23] Cardoni, J. N., and Rizwan-uddin. "Nuclear Reactor Multi-Physics Simulations with Coupled MCNP5 and Star-CCM+." *International Conference on Mathematics and Computational Methods Applied to Nuclear Science and Engineering*, (2011).

[24] Christon, M. A., J. Bakosi, M. M. Francois, R. B. Lowrie, R. Nourgaliev. "Multiphase Flow Analysis in Hydra-TH." *Conference: CASL Virtual Roundtable*, (2012).

[25] Sussman, M., A. S. Almgren, J. B. Bell, P. Colella, L. H. Howell and M. L. Welcome., "An adaptive level set approach for incompressible two-phase flows.", *Journal of Computational Physics*, Vol. 148, Issue 1, 81-124 (1999).

[26] Popinet, S. and Zaleski S. "A Front-Tracking Algorithm for the Accurate Representation of Surface Tension." *International Journal of Numerical Methods in Fluids*, Vol. 30 No. 775, (1999).